Excitation Emission Matrix (EEM) Spectroscopy and Computational Evaluation of Excited States of Carbazole – Bromobenzothiadiazole (CBB)

By

Sara Joulaei Zonouz

B.Sc. Applied Chemistry, Sharif University of Technology 2020

A thesis submitted in partial fulfillment of the requirements for the degree of

MASTER OF SCIENCE

in the Department of Chemistry

University of Victoria

Excitation Emission Matrix (EEM) Spectroscopy and Computational Evaluation of Excited States of Carbazole – Bromobenzothiadiazole (CBB)

By

Sara Joulaei Zonouz

B.Sc. Applied Chemistry, Sharif University of Technology 2020

Supervisory Committee

Dr. Hans-Peter Loock, Supervisor

Department of Chemistry

Dr. Heather Wiebe

Department of Chemistry

Abstract

We examine the source of solvatochromism in a fluorescent organic dye using fluorescence Excitation Emission Matrix (EEM) spectroscopy, supported by ab initio calculations. The dye, carbazole–bromobenzothiadiazole (CBB), has a donor-, an acceptor-, and a bridging group connected by sigma bonds. The study of its fluorescence in liquid solutions shows a strong emission wavelength dependence on the solvent polarity but only a negligible dependence on solvent viscosity. In previous work, the polarity-induced solvatochromism was attributed to a twisted intermolecular charge transfer (TICT) state, where the excited state twists into a conformation in which a large dipole is generated between the carbazole (donor) group and the benzothiadiazole (acceptor) group. (1)

Density Functional Theory (DFT) calculations are performed to map the excited state potential energy surface and the associated dipole moment in different solvent environments using the corrected linear response (cLR) solvent model (2). The calculations agree well with the observed energy differences and the solvatochromic shifts.

To determine the configuration of the molecule in the excited state before emission, the dihedral angles between the three main groups of the molecule are investigated. Ab initio calculation indicates that the three dihedral angles between the donor-, bridging-, and acceptor-groups in the excited state change only by comparably small amounts between the Franck-Condon region and the potential minimum of the excited state, from which fluorescence is expected to occur. The molecular configuration in the excited state's potential minimum is therefore close to the molecular structure in the Franck-Condon region, and not a "twisted" structure indicative of a TICT structure. Interestingly, we calculate a second local minimum on the excited state in the global excited state form when the third dihedral angle, θ_3 =90°. However, the energy in this twisted form is much higher than that of the first minimum configuration (θ_3 = 0°). Since the second excited state minimum is not accessible upon excitation of the molecule emission is calculated to occur from the lowest excited state, which was, indeed, observed. Consequently, in this research, the solvatochromic shift is due to the charge separation around the acceptor domain, which is partially induced by the polarity of the environment.

This work raises questions about the presence of TICT state in other molecules. We argue that the observation of solvatochromatic shifts, and the presence of donor and acceptor moieties alone are not sufficient to positively identify a TICT state.

We found that TD-DFT calculation require a sophisticated solvent model to quantitatively model the solvatochromic shift. Also, we observed the natural transition orbitals are far more useful in identifying donor and acceptor moieties compared to the commonly used canonical orbitals. Excitation Emission Matrix (EEM) spectroscopy serves as a useful experimental tool to identify excitation and emission pathways.

Table of contents

List of Figures

List of Tables

List of Abbreviations

CAM-B3LYP	correlation functional using the Coulomb-attenuating method in B3LYP
CBB	Carbazole–Bromobenzothiadiazole
CC	Coupled-Cluster
CI	Configuration Interaction
cLR	Corrected Linear Response
CT	Charge Transfer
DFT	Density-Functional Theory
DZ	Double zeta
EEM	Excitation Emission Matrix
ET	Electron Transfer
FK	Franck-Condon
HF	Hartree-Fock
HK	Hohenberg and Kohn
ICT	Intermolecular Charge Transfer
KS	Kohn-Sham
LE	local Excited State
L-M	Lippert-Mataga
LR	Linear Response
MP	Møller-Plesset perturbation theory
NTO	Natural Transition Orbitals
OLEDs	Organic Light-Emitting Diode
PCM	Polarized Continuum Model
PEG	Polyethylene Glycol
PES	Potential Energy Surfaces
PMT	Photomultiplier Tube
RCAM-B3LYP	Restricted CAM-B3LYP
RSS	Residual sum of squares

SCF	Self-Consistent Field
SS	State-Specific
STOs	Set of Slater-type Orbitals
TD-DFT	Time-Dependent Density Functional Theory
TICT	Twisted Intermolecular Charge Transfer

Acknowledgment

I would like to express my heartfelt gratitude to my supervisor, Dr. Hans-Peter Loock, for his unwavering support and trust. Despite the distance between us during our initial virtual conversation, he welcomed me into his research group in Canada. His enthusiasm and assistance have been crucial to completing this project over the past two years. I will always be grateful for these priceless contributions and for making a peaceful environment for the group. In addition, special thanks to Dr. Heather Wiebe, who helped in computational calculation a lot, nice to meet you in GSRD.

My special appreciation goes to Erin Hodgson, who has been by my side from the day I was admitted to UVIC until the defence. I am grateful for her patience and support.

I express my deep gratitude to all the Loock Laser Lab group members. Oren, thank you for guiding me through my first year at UVIC. Monique, Emma, and Swapnil, your support and willingness to listen to my concerns during challenging times have meant the world to me. Dr. Chris Prüfert, thank you for your technical assistance during the more complex aspects of the project and edition of this thesis. Arthur and Yasaman, having you in our group has been a pleasure.

A special thanks go to Nikoo, my friend, my previous classmate in my bachelor and my roommate because of all the days being next to me. Thanks for making life easier, far from home. I would also like to thank Yasaman, and Afsaneh, as spending weekends with you exploring the island brought great joy.

Finally, I want to dedicate a special thanks to my family. To my dad, who has always been my pillar of support, I am certain that none of this would have been possible without you, to my mom, who resides in my heart every moment, and my beloved sister, Homa. Although I am far from home, my heart is always with you.

This project is dedicated to the memory of Dr. Erin Chernick, who designed the carbazole–bromobenzothiadiazole organic compound and allowed us to research it. Dr. Chernick was an Assistant Professor in the Department of Chemistry, and her untimely passing in May 2022 at the age of 41 was a profound loss.

Chapter 1: Introduction

When organic chemists design molecules, they have their particular use in mind. Some are designed to have a biological effect, either by reacting with other compounds in a body or, more typically to attach physically to biological binding sites, Others act as surfactants, as molecular "shuttles", as coatings, or as catalysts to accelerate reactions. Fluorescent organic molecules are a thoroughly studied group of molecules that emit light when excited with light of a shorter wavelength (higher energy). They can be deployed as molecular "beacons", or fluorescent tags, but also can be designed to change their light emission when their local environment is changed. There are many advantages in using fluorescence as a reporter of the physical environment. Excitation and emission of light can be done remotely over long distances, as long as the medium is transparent to the excitation and emission of light. The process is non-destructive, i.e. the same molecule can be used for a long time. The process can be made very efficient, such that a fluorescence photon is emitted almost every time an excitation photon is absorbed. Most importantly, fluorescence labels have molecular dimensions allowing us to probe micro-environments on a near-length scale that is comparable to the size of the molecules (3-6). Several Nobel Prizes were awarded recently for the study of fluorescence properties and for identifying new applications. The 2008 Nobel Prize in Chemistry was awarded jointly to Martin Chalfie, Osamu Shimomura and Roger Y. Tsien, "for the discovery and development of the green fluorescent protein, gfp". The Nobel Prize in Chemistry 2014 was awarded jointly to Eric Betzig, Stefan W. Hell and William E. Moerner "for the development of super-resolved fluorescence microscopy". Most recently, the Nobel Prize in Chemistry 2023 was awarded to Moungi Bawendi, Louis Brus and

Aleksey Yekimov “for the discovery and synthesis of quantum dots.”, small particles that are noted for their size-dependent fluorescence properties (6, 7)

Fluorescent molecules have been crucial in analyzing local chemical environments since they provide information on the physical characteristics of the environment that they reside in, such as viscosity, polarity, pH, temperature, and pressure. Twisted-internal charge transfer (TICT) states, which are present in a unique class of fluorescent compounds, have attracted particular interest because of their unique properties. These states are considered ideal candidates for the investigation of complex microenvironments because they exhibit variations in fluorescent wavelength with solvent polarity and fluorescence intensity with solvent viscosity (8-10).

The unique properties of TICT states are caused by the presence of electron donor and acceptor groups in a molecule, which, upon excitation, may lead to charge separation in the electronically excited state. This strongly dipolar excited state is stabilized in polar solvents, resulting in a bathochromic fluorescence shift “red-shift” when compared to their solutions in non-polar solvents. Additionally, significant Stokes shifts are often observed in molecules that emit from TICT states, indicating that the minimum potential energy region of the excited state potential surface is well below the energy of the locally excited state. Many authors have described the motion of the molecule in the excited state as a twisting motion around the σ-bond that connects the donor and acceptor groups. The respective dihedral angle becomes therefore an important reaction coordinate (11).

In the electronic ground state, these molecules often exhibit a dihedral angle around 0^0, facilitated by π-conjugation between the donor- and acceptor groups (12). In the absence of this conjugation, the dihedral angle can assume a range of values, and typically assumes high angles due to steric hindrance between substituents on the donor and acceptor groups. Upon excitation, fluorescence

from both local minima is sometimes observed; emission from the local excited, LE, state potential minimum near the ground state angle competes with emission from a twisted, electron-transfer configuration, ET. The relative contribution of the near-planar configuration and the twisted configuration to the emission spectrum depends on the balance between steric hindrance and electron delocalization (12). The significance of the solvent environment becomes evident as the twisted configuration is strongly dipolar and is stabilized by polar solvents, resulting in a strongly solvatochromic fluorescence emission. Molecules with TICT states are designed to contain some steric bulk to lower the energy barrier to the twisted conformation. Large substituents on the donor and acceptor groups repel each other, thereby creating an energy barrier in the co-planar conformation of the donor and acceptor groups. In viscous solvents, where high solvent viscosity hinders the formation of the twisted configuration, the dominant fluorescence intensity is from the ^{1}LE state. By contrast, in less viscous solvents, weaker yet strongly solvatochromic fluorescence from the ^{1}ET state is observed (13).

Our understanding of these phenomena was generated from 30+ years of experimental and theoretical studies of TICT states, which have also been introduced as useful tools for measuring the polarity and viscosity of local solvents. TICT molecules can work as reliable probes for these physical characteristics if one tracks the ratio of electron transfer state (ET) and local excited state (LE) fluorescence or monitors the overall fluorescence intensity (12, 14). Strong donor and acceptor groups are often featured in these molecules, and bridge moieties may be introduced to create additional dihedral angles (13).

In the past, TICT states have been identified through their distinctive characteristics, including dual fluorescence emissions, a significant Stokes shift, and a bathochromic response of the ET minimum in polar liquids (12, 15). These experimental observations have often been substantiated using

calculations of frontier orbitals, particularly the highest occupied molecular orbital (HOMO) and the lowest unoccupied molecular orbital (LUMO). The present study challenges the conventional approach by presenting a molecule that exhibits typical TICT-state behavior, such as strongly Stokes-shifted fluorescence emission and strong solvatochromism, without possessing a dipole along the donor-acceptor axis or even undergoing the requisite electron transfer.

In this work the absorption and excitation-emission matrix (EEM) spectra of a previously identified molecule in several solvents are provided, adding to the body of experimental knowledge about this substance. Then, to calculate Stokes shifts and solvatochromic shifts, a multi-step computational method that involves computing sections of the excited state potential energy surface is used. Our results agree very well with the experimental evidence and both methods show almost the same solvatochromic shift due to changing the polarity of the environment.

Considering the molecule's frontier and natural transition orbitals, the findings are interpreted. Accordingly, a TICT state minimum is identified in a region of the excited state potential surface that is inaccessible from the Franck-Condon region. The molecule would have to cross a high energy barrier to reach the TICT state. The TICT state minimum is calculated to be situated in an area of the excited state potential surface and is only present in strongly polar solvents.

In conclusion, the complexity of TICT states and their utility for analyzing local chemical environments is explored in this work. We aim to deepen the understanding of these fascinating events and contribute to the creation of novel molecules intended for environmental probes. This is achieved by questioning established practices and introducing a more comprehensive approach to TICT state characterization.

The format of this thesis is as follows:

In Chapter 2, the theoretical foundations for the present are discussed, and the definitions for all the concepts to be addressed in the following chapters are provided.

In Chapter 3, the experimental and computational processes are detailed, and the resulting data is reported. Finally, Chapter 4 involves the analysis of the results to arrive at a conclusion regarding the project.

The work contained within this thesis was presented at the Canadian Chemistry Conference and Exhibition in Calgary, Canada in June 2022 and Vancouver, Canada in June 2023. This project was also showcased at the 2023 Graduate Student Research Day at UVic and canPOM 2022 online meetup. A publication containing a substantial fraction of the data presented in this thesis is currently under review by the *RSC New Journal of Chemistry*.

Chapter 2: Theoretical Background

2.1 Fluorescence

2.1.1 Fluorescence Mechanism

All molecules contain higher electronic states in addition to their ground electronic state, E_0. These states arise when one or more electrons are promoted from an occupied molecular orbital to an empty orbital at higher energy. When a photon with energy equal to the difference between the two electronic states interacts with the molecule, an electron is excited from the occupied orbital to a higher-energy orbital. In general, when a molecular species undergoes excitation to a higher energy state consequent to the absorption of light, the system can discharge the excess energy through diverse pathways. These pathways encompass the emission of electromagnetic radiation, redistribution of energy across internal degrees of freedom within the molecule, interaction through collisions with other molecules, or, under extreme circumstances, dissociation into atomic and/or molecular fragments. The light emission process is called "fluorescence" when the excited molecules emit light upon relaxing to the ground electronic state without changing the total electron spin. Compared to the excitation wavelengths, the fluorescence wavelengths are longer (corresponding to lower photon energy), since some of the excitation energy is converted into internal energy, in a process called vibrational relaxation or "internal vibration redistribution (IVR)" (16).

The Jablonski diagram illustrates schematically the possible processes that follow the absorption of a photon. Aside from the process described above, the diagram also shows the internal conversion of a higher-lying S_2 state to the S_1 state from which fluorescence can occur. Kasha's rule states that *any* higher-lying state will first convert to the lowest-lying, S_1 singlet state before fluorescence is observed (17). Triplet states are present for any excited state singlet states and lie below the respective singlet states by an amount corresponding to the spin-orbit coupling energy (typically 0.5 eV or less). Conversion into triplet states and light emission (phosphorescence) from triplet states to a (singlet) ground state is spin-forbidden. The number of phosphorescent molecules is therefore much smaller than those of fluorescent molecules (Figure 1)(18).

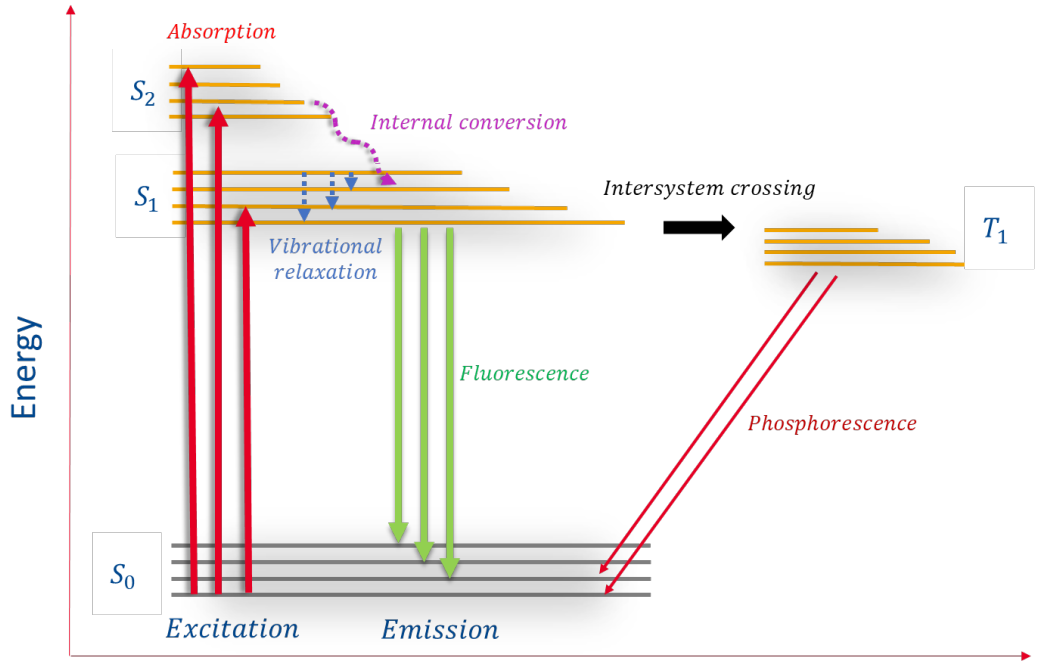

Figure 1 A Jablonski diagram(19)

2.1.2 Fluorescence Spectroscopy

Fluorescence spectroscopy can be used to analyze chemical samples based on features in their fluorescence spectrum. In this method, the sample containing fluorescent compounds is excited by a light source and the emitted light is detected. The excitation spectrum of a fluorescent molecule is frequently quite similar to the absorption spectrum – it would be identical if the quantum yield, i.e. the fraction of excitation photons converted into fluorescent photons, does not depend on the excitation energy. The emission spectrum depends on the amount of energy lost non-radiatively, the Stokes shift. Both spectra are shaped, in addition, by the shape of the potential energy surfaces of the respective ground state and excited state.

Fluorescence Spectrometers are designed to meet the requirements of the desired application. Depending on the application a fluorimeter can be designed to provide high spectral resolution, high time resolution, high spatial resolution, or a combination of these parameters. All fluorometers measure the emitted light spectrum using a photodetector. Fluorescence spectrometers typically consist of a light source, a dispersive element to select the desired excitation and/or emission wavelength, and a detector (16, 20).

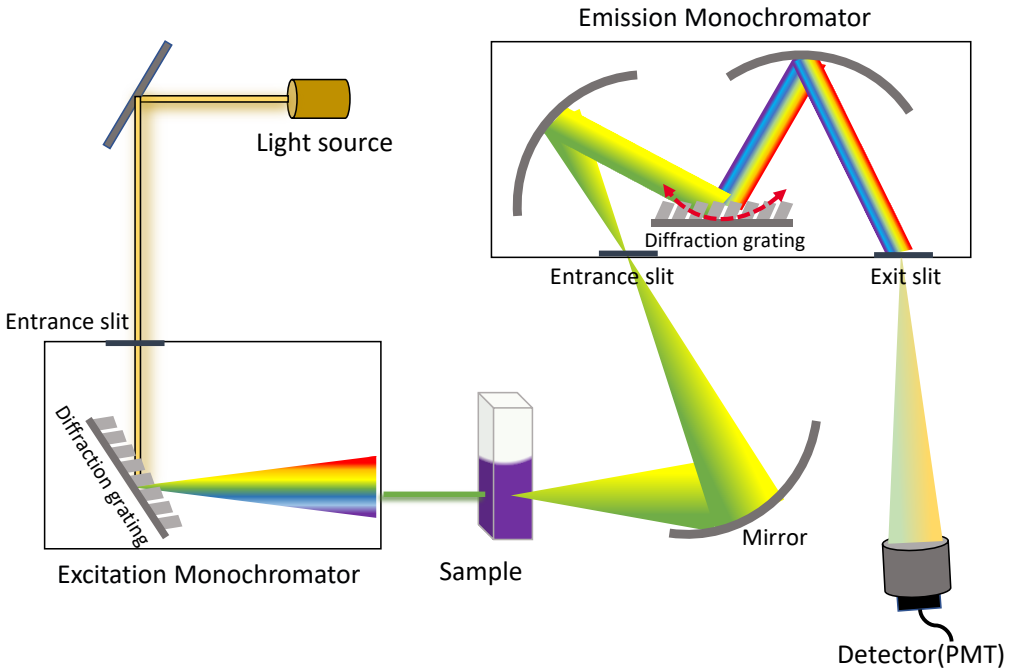

Figure 2 Diagram of a typical Fluorescence Emission Spectrometer having a fixed excitation wavelength (21)

Light sources provide light for exciting the sample and they are selected based on the application and desired wavelength. There are different light sources like xenon lamps, high-pressure mercury lamps, quartz-tungsten, halogen lamps, LED light sources and lasers. The light of most sources covers a broad range of wavelengths from which a small portion may be selected using a dispersive optical element. Filters and monochromators are the most common dispersive elements with filters being much simpler in comparison to monochromators. Many filter-based fluorometers use two filters: one to select the excitation wavelength and a second for the emission wavelength. For monochromator-based instruments, two diffraction grating are used to select the desired excitation and emission wavelengths. The monochromators act as tunable, narrow-band (2-5 nm) band-pass filters. Here, the emitted light from the sample is transmitted to a broadband detector to record (Figure 2)(20).

Photomultiplier tubes (PMTs) can detect photons with wavelengths between 120 nm to 1100 nm. A PMT is a single-pixel detector which can be configured to detect individual photons. PMTs currently have the best single-wavelength detection performance, with regard to sensitivity and stability, signal-to-noise ratio, and time resolution. Photomultiplier tubes can be purchased for

different wavelength ranges, different light intensity ranges, and different application conditions (20).

Today, fluorescence spectroscopy instrumentation is used in multiple applications including chemistry, biochemistry, medical research, pharmaceuticals, food science, environmental studies, and nanotechnology.

2.1.3 Fluorescence lifetime

Fluorescence lifetime is the time a fluorophore spends in the excited state before emitting a photon and returning to the ground state. A typical fluorescence lifetime is near 10 ns (10×10^{-9} s) for many fluorophores but it varies across orders of magnitude depending on the type of compound, their excited state, and the fluorophore's environment There are three steps which govern the fluorescence process. The excitation of a molecule by a photon happens in femtoseconds (10^{-15} seconds), vibrational relaxation of excited state electrons to the lowest energy state is much slower and happens in picoseconds (10^{-12} seconds) and the molecule returns to its ground state and emits a longer wavelength photon in the nanosecond time scale (10^{-9} seconds). Phosphorescence happens on a much longer time scale (microseconds:10^{-6} s) and is governed by the rate at which a spin-flip in a formally spin-forbidden transition can take place (16). Due to the significant discrepancy in speed between electronic excitation and the motion of atomic nuclei, it is often feasible to mathematically separate these processes. This fundamental concept is known as the Franck-Condon approximation. This approximation allows us to conveniently calculate the excitation energy at a specific, fixed molecular geometry, typically at the ground state potential energy minimum. In this context, it simplifies the mathematical treatment of electronic transitions by assuming that nuclear motion is negligible during the electronic excitation process (22).

The Franck-Condon principle states that the excitation time to a higher electronic energy level for the fluorophore in the solvent is shorter than the time in which the solute and solvent need to rearrange. For this reason, the reorientation of the solvent in the presence of a changed solute molecule with a different dipole moment happens with a delay after excitation. Following excitation, the fluorophore will change its conformation towards the minimum of the excited state

potential in a process that takes picoseconds to nanoseconds. At the same time, the solvent molecules reorient themselves (22, 23).

The properties of a fluorophore in its excited state, such as dipole moment, acidity, nucleophilicity or electrophilicity, can be entirely different from the ground state, and as a result, it will interact differently with its environment. For example, the fluorophore's molecular dipole moment always changes upon excitation, which causes the rearrangement of solvent molecules. While the molecule moves towards the excited energy minimum and the solvent molecules adjust accordingly, some of the excess nuclear energy is also distributed to the solvent environment, i.e. the fluorophore relaxes vibrationally so that in the excited state equilibrium most vibrational modes are thermally equilibrated. Emission then occurs from the minimum of the excited state potential surface. Of course, the fluorophores' interaction with solvent molecules affects fluorescence emission wavelength due to the solvent polarity. Solute-solvent Interactions that take place in the local environment during the excited state lifetime cause a large portion of the fluorescence sensitivity (24).

2.1.4 Kasha's Rule

Kasha's rule is one of the main principles of spectroscopy. Kasha's rule is best stated exactly as it was by Kasha:

"The emitting level of a given multiplicity is the lowest excited level of that multiplicity (25)."

Therefore, Kasha's rule states that fluorescence will always originate from the vibrational level of the lowest excited state of the singlet level, S_1, regardless of the initial state that had been excited (17).

2.1.5 Stokes shift

When a system (be it a molecule or atom) absorbs a photon, it gains energy and enters an excited state. One way for the system to relax is to emit a photon, thus losing its energy (another method would be the loss of energy as translational mode energy via vibrational-translational or electronic-translational collisional processes with other atoms or molecules). The wavelength difference between light that is absorbed and light that is emitted when a molecule fluoresces is

referred to as the Stokes shift. A molecule that absorbs a photon usually transitions to an excited state and then after losing a small amount of energy through vibrational relaxation releases a longer wavelength photon, to return to the ground state, which is a lower energy state. The Stokes shift is the wavelength difference between the light that is absorbed and that is emitted (Figure 3) (26).

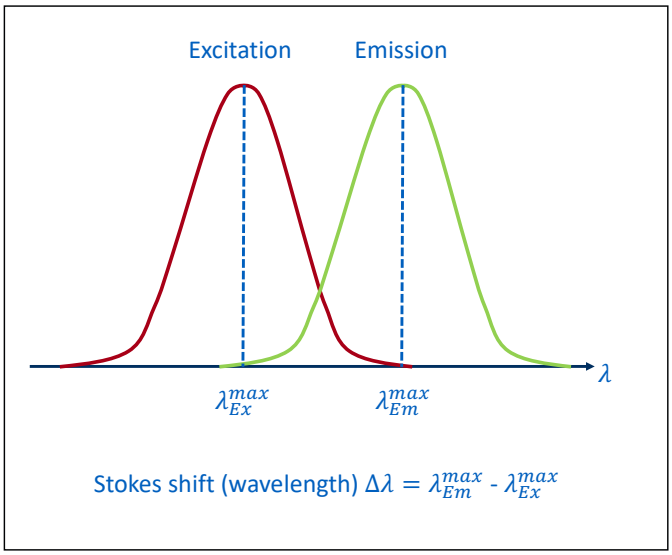

Figure 3 Stokes shift in fluorescence spectroscopy

The extent of the fluorescence's stokes shift depends on the fluorophore and its environment. In the presence of the polar solvent, the fluorophore's excited state would be more stable and emit light with a lower energy. Therefore, polar solvents cause longer fluorescence emission wavelengths than non-polar solvents. This effect is called solvatochromism (27).

2.1.6 Fluorescence Excitation Emission Matrix Spectroscopy

Excitation Emission Matrix (EEM) spectroscopy is a type of fluorescence spectroscopy that measures the fluorescence intensity of a sample over a range of excitation and emission wavelengths. The spectroscopic data is plotted as a three-dimensional surface, with the excitation and emission wavelengths on the x and y axes, respectively, and the fluorescence intensity on the z-axis. A typical Excitation Emission Matrix (EEM) is shown in Figure 4.

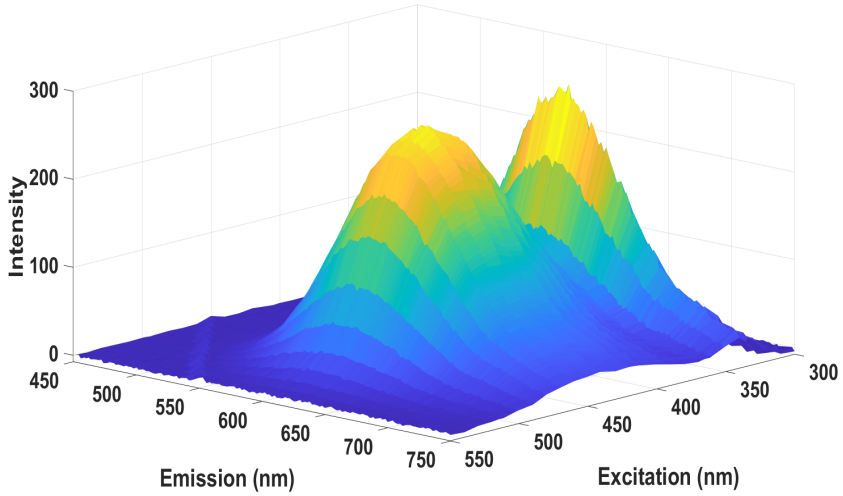

Figure 4 Excitation Emission Matrix of CBB

One typical EEM spectrometer is shown in Figure 5. It included two monochromators; the first one is the excitation monochromator which disperses white light from the source. A diffraction grating in the excitation monochromator is rotated to scan the excitation wavelength during the acquisition of an excitation spectrum and passes the desired wavelength through the slit to the fluorescent sample. The emission light from the sample is collected at 90°. The emission light is pass through the entrance slit to enter the emission monochromator. The grating in the emission monochromator is rotated to scan the emission wavelength during the acquisition of an emission spectrum. Scanned emission light passes to the broad-band detector through an exit slit and is recorded by the detector. EEM spectroscopy is advantageous compared to fluorescence detection with a single excitation wavelength when there are multiple possible fluorophores in a sample. The EEM spectrum provides a spectral fingerprint of the sample that would allow the user to either identify the fluorescing compounds by its unique EEM spectrum or even distinguish several fluorescing compounds following multivariate analysis (28).

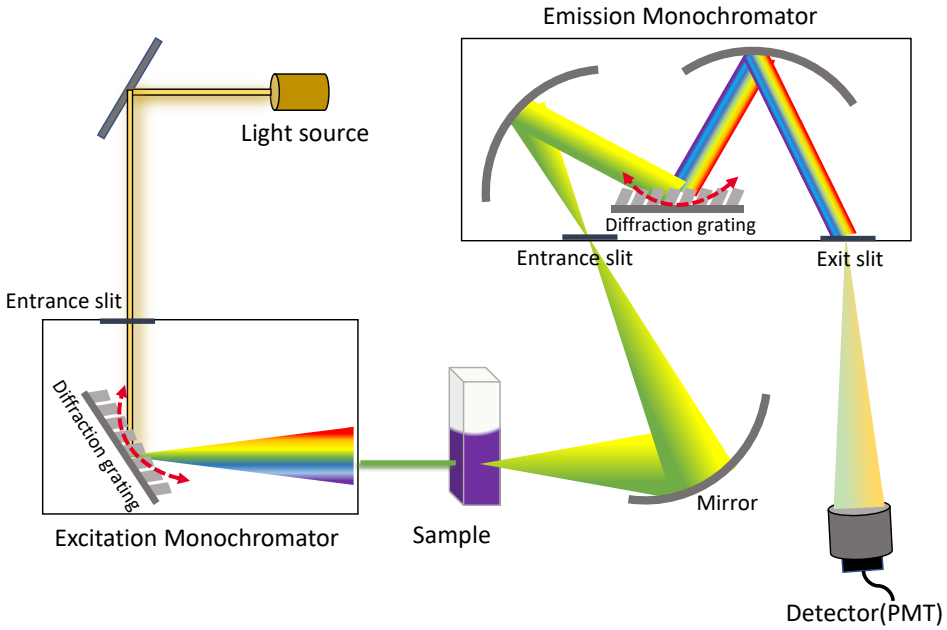

Figure 5 Excitation Emission Matrix Spectrometer-Excitation and Emission wavelength both are scanned with diffraction grating rotation (that figure is similar to Figure 2 but the diffraction gratings in both excitation and emission monochromators are rotating in here)

2.1.7 Fluorescent organic probes

An organic compound has colour because:

a. absorbs light in the visible spectrum (400 -700 nm)

b. has at least one chromophore in its structure for example the part of a molecule that gives it colour like the retinal in the eye to detect the colour

c. has a conjugated structure

d. demonstrates electron resonance, which serves as a stabilizing force in organic compounds (29)

Organic dyes are commonly used as pigments to make e.g. colourful paper, leather, and plastics. They also form the basis of organic light emitting diodes (OLEDs), and dye-sensitized photovoltaic cells. Their use as chemical sensors is most important in this work. Chemical sensors react to their environmental changes; here dyes can change their colour in response to their surrounding medium. Temperature and viscosity, or polarity changes in the solvent environment are examples of environmental changes. The process of changing the colour of the compound is called chromism (30) (31) and accordingly dyes whose colour could change due to the change of the solvent are

called solvatochromic dyes. Rhodamine B is a popular dye for chemists because of its solvatochromic features. Figure 6 presents Rhodamine-B fluorescence behaviour in the presence of different solvents. Solvatochromic dyes exhibit different excitation and emission spectra depending on the environment's polarity.

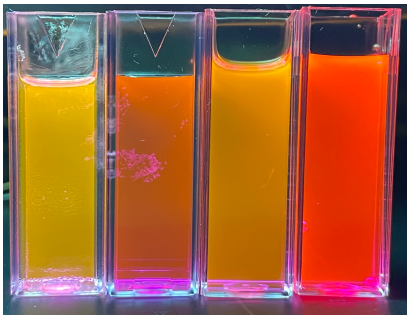

Figure 6 Rhodamine. B in chloroform, de-ionized water, ethanol and glycerol exposed to 365 nm UV light

Another kind of fluorescence dye is called fluorogenic dye; its fluorescence *intensity* changes upon interaction with other chemical groups. For example, the viscosity of the solvent environment can affect the fluorescence intensity of this kind of dye. Figure 7 shows the functional difference between the two types of dyes on the fluorescence spectrum.

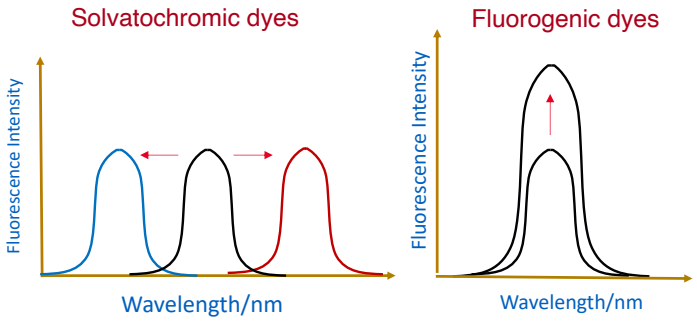

Figure 7 Fluorescence spectrum changes of solvatochromic due to polarity changes and fluorogenic dyes by changing the environment viscosity(32)

Solvatochromic dyes and fluorogenic dyes are environment-sensitive probes that play a crucial role in fluorescence sensing and imaging. Fluorescence microscopy is an imaging technique that utilizes fluorescent dyes to provide insights into microenvironmental changes in biological samples (32) and is one of the main applications of fluorogenic and solvatochromism dyes, as their fluorescence response can provide chemical information or their local (micro) environment.

In this project, carbazole–bromobenzothiadiazole (CBB) is investigated as an organic dye showing strong solvatochromic and fluorogenic properties (1).

2.2 Computational Chemistry

Computational chemistry is an area of study that combines principles of chemistry, physics, and computer science. It seeks to comprehend the behaviour and characteristics of molecules, groups of molecules, and solid materials using various computational techniques and algorithms. In this work, computational chemistry is a useful tool for predicting fluorescence energies and comprehending the electronic characteristics and behaviour of molecules in their excited states. Using high-level computational approaches researchers can identify the molecular structure, electronic transitions, and excited state dynamics that affect fluorescence by using a variety of computational techniques.

In computational chemistry, there are two methods for modelling spectroscopic features: the semi-empirical method and the *ab initio* method. The *ab initio* technique uses the Schrödinger equation without any additional experimentally obtained approximations. The semi-empirical method is based on both empirical (experimental) input and quantum mechanics. Both methods involve approximations leading to errors in the results, and computational chemistry aims to reduce this error as much as possible. The *ab initio* method uses only Schrödinger's equation ($E\Psi = H\Psi$) and atomic properties as an input and can be more accurate than the semi-empirical method – especially for small molecules having only a few electrons. On the other hand, *ab initio* can be extremely time-consuming and inaccurate for larger molecules or complicated electronic structures (33). The evaluation of large molecules then requires supercomputers with large CPUs to complete the calculation in a reasonable time. In this project, all computational *ab initio* calculations are done using the *Gaussian 16* software package with support provided by BC DRI Group: University of Victoria and the Digital Research Alliance of Canada (alliancecan.ca).

2.2.1 Hartree-Fock Approximation

The typical method for solving a quantum chemistry problem is to use the electronic Schrödinger equation. The Schrödinger equation can only have exact solutions for one-electron chemical systems. As a result, one can only use approximations when solving many-body issues. The

Hartree-Fock technique is one of several approaches employed in quantum chemistry to approximate solutions to the Schrödinger equation. The Hartree-Fock (H-F) wave function is the ideal wave function with orbitals assigned to electrons. The Hartree–Fock orbitals ϕ_i of a molecule must be found by solving the Hartree–Fock equations(33):

$$\hat{F}\phi_i = \varepsilon_i\phi_i \qquad 1$$

where the Hartree–Fock operator $\hat{F}$ is an operator based on the Hamiltonian operator. Each of the spatial orbitals ϕ_i is a function of the three spatial coordinates; ε is the energy of orbital *i.* The operator $\hat{F}$ is a special mathematical operator that depends on ϕ_i. We discover the form of $\hat{F}$ when we solve the H-F equation. It's important to note that $\hat{F}$ is not truly "unknown" but rather becomes clear through solving the equation. The $\hat{F}$ is ultimately obtained through an iterative process from the electron-electron interactions and the many-electron wave function. A set of optimized one-electron wave functions, or orbitals, that minimize the system's energy are obtained by building the $\hat{F}$ using the Hartree-Fock equations, which represent a self-consistent field (SCF) approach. To solve these equations, we make an initial guess for the orbital ϕ_i which is usually based on a weighted sum of pre-determined atomic orbitals. By this initial guess, we can calculate an approximate form of $\hat{F}$. Then, we use this approximate $\hat{F}$ to solve the equations again, resulting in a better set of eigenfunctions. This process is repeated, using the improved eigenfunctions to calculate an even better $\hat{F}$, and so on. This process is continued until the eigenfunctions do not change significantly from one iteration to the next. This is why this method is called the “self-consistent field” (SCF) method.

The most convenient way to express Hartree–Fock orbitals is as a linear combination of n one-electron wave functions called basis functions where this set of functions is a complete orthonormal set, i.e. the wavefunction can be used to construct all molecular wavefunctions. The set of Slater-type orbitals (STOs) is a complete set of basis functions frequently employed in atomic and molecular Hartree-Fock calculations. One drawback of H-F calculations is that they do not account for electron correlation, so H-F only considers the average effect of electron repulsion, but not the explicit electron-electron interaction. Due to the H-F theory, the possibility of discovering an electron at a particular location near an atom is affected by its distance from the nucleus, but not by that of other electrons. Physically, this is not accurate, but it is a result of the

central field approximation, which characterizes the H-F method. As a result, between the calculated energy using the Hartree-Fock method and the actual energy, there is some difference. Neglecting electron correlation can cause large deviations from experimental results. Configuration interaction (CI), coupled-cluster (CC), Møller-Plesset perturbation theory (MP) and Density-Functional Theory (DFT) are different methods that begin with H-F calculation and are corrected for correlation. In addition to being reasonably precise, DFT is also computationally more efficient than many other methods, especially for systems with plenty of electrons (33).

2.2.2 Basis sets

A basis set is a combination of functions used to describe atomic and molecular orbitals. The smallest basis set used to describe an atomic orbital is called the minimal basis set. For each atomic orbital in the inner shell and the valence shell of this basis set, just one Slater-type orbital (STO) is used. However, these minimal basis sets are not adaptable enough to accurately represent orbitals or describe how electrons are distributed among nuclei to form chemical bonds. So-called double zeta (DZ) basis sets are employed to increase flexibility, with two basis functions corresponding to each valence atomic orbital. Since the different orbitals of the "split-valence" basis functions have varying spatial extents, this combination allows the electron density to adjust its spatial extent appropriately to the molecular environment. That is, the value of ζ accounts for the size of the orbitals.

Even though STOs are frequently used as basis sets in atomic calculations, using STOs as basis functions in calculations involving polyatomic molecules results in integrals that take a long time to compute on a computer. As a result, the basis functions for most molecular quantum-mechanical calculations are Gaussian functions rather than STOs. Since a single Gaussian-type Orbital, GTO, function is not appropriate for describing atomic orbitals, a linear combination of several Gaussian functions is used as the basis function instead of using individual Gaussian functions. There are numerous Gaussian basis sets that can be used in molecular calculations. The basis sets created by Pople and colleagues are some of the most widely used. Some examples of these basis sets are the 3-21G, 3-21G(p), 6-31G(p), 6-311G(p), and 6-31G(p,d) sets, where the numbers and symbols are related to the number of Gaussian functions on each atom (33-35) .

2.2.3 6-31G+pd basis set

The 6-31G basis set and its variations are one of the most widely used basis functions of the Pople basis sets. These sets employ a split-valence strategy, with one basis function for each core orbital (6) and two basis functions (31) for each valence orbital. This configuration makes it possible to represent the behaviour of electrons in molecules.

Additional basis functions have been added to enhance the description of molecular systems. Polarization basis functions, denoted as (d) or (d, p), account for changes in electronic charge during chemical bond formation. They offer flexibility in describing electron redistribution and have higher angular momentum than the valence orbitals. Conversely, diffuse functions enhance the realistic representation of electron behaviour in the outer regions by capturing electron density far from the nucleus (36).

2.2.4 Density Functional Theory

Density Function Theory (DFT) is based on a theorem proved in 1964 by Pierre Hohenberg and Walter Kohn (H-K) (34). The required time to perform a DFT calculation is the same as that for a Hartree-Fock function on the same molecule with the same basis set. The Hartree-Fock calculation results in a wave function with an estimated energy while DFT determines energy and other molecular properties. In the DFT method, the molecular wave function is not calculated. Instead, all properties of the molecular systems in their electronic ground state can be determined by their electron density ρ(x,y,z). One therefore says that the ground state electronic energy E_{gs} is a functional of ρ and one writes (33):

$$E_{gs} = E_{gs}\left[\rho\right] \qquad 2$$

Where the square brackets denote a functional relation. To understand the difference between a function and a functional, consider this analogy: a function $y = f(x)$, is a mathematical rule that connects a number (the value of y) to a specific value of the independent variable x. On the other hand, a functional $z = G[f]$ is a rule that associates a numerical outcome with a whole function, not just a specific input. In simpler terms, a function gives you a number for a

given input, while a functional gives you a number for an entire function. Unfortunately, the functional $E_{gs}[\rho]$ is unknown, so the Hohenberg-Kohn theorem does not tell us how to calculate E_{gs} from ρ or how to find ρ without first finding the ground-state molecular electronic wave function. In 1965 Walter Kohn and Lu Jeu Sham (Kohn-Sham, K-S) introduced a method for more accurate calculation of molecular properties (33).

The K-S method has a fictitious reference system with an electron number that is the same as that of the desired molecule, but there are no forces between the electrons in the reference system. Since each electron in the reference system experiences the same potential energy, the electron probability density in the reference system is exactly equal to the ground-state electron probability density in the actual molecule.

So, the K-S equation to the molecule's ground-state electronic energy is equal (33):

$$E_e = \langle K_{es} \rangle + \langle V_{Ne} \rangle + J + V_{NN} + E_{xc}[\rho] \qquad 3$$

Where $\langle K_{e,s} \rangle$ is the average electronic kinetic energy in the reference system, V_{Ne} is the average potential energy of attractions between the electrons and the nuclei in the molecule, J is the classical energy of electron repulsion that arises between the infinitesimal charge elements of a hypothetical smeared-out electron charge cloud whose probability density is $\rho(x, y, z)$, V_{NN} is the internuclear repulsion energy and $E_{xc}[\rho]$ is exchange-correlation energy functional**.** The exchange operator is present to make the overall wave function antisymmetric with regards to the exchange of electrons and involves only the occupied orbitals. This functional provides a correction for those instant correlations between electron movements that cause correlation effects on the energy. $E_{xc}[\rho]$ itself is a function of the electron density $\rho(x, y, z)$. It is defined as (33):

$$E_{xc}[\rho] \equiv \langle K_e \rangle - \langle K_{es} \rangle + \langle V_{ee} \rangle - J \qquad 4$$

Where $\langle K_e \rangle$ is the average electronic kinetic energy in the molecule and $\langle V_{ee} \rangle$ is the average potential energy of interelectronic repulsion.

One of the main challenges of the DFT calculations is finding the appropriate functional for each molecule. Hybrid functionals are a class of approximations to the exchange–correlation energy functional DFT that combines the exchange-correlation energy from other sources (*ab initio* or empirical) with a portion of the exact exchange from the Hartree-Fock theory.

The most common model for hybrid functions is B3LYP. In this function, B indicates that it includes a term by Becke, LYP is a term which is introduced by Lee, Yang, and Parr and it has three empirical parameters whose values were chosen to optimize its performance. There is not a definitive "best" function. A functional may be effective for calculating the energy level in a particular class of molecules, but it may have a large error in calculating another property or on another group of molecules. The appropriate function is obtained by trial and error (33).
For measuring excited state energy, we use the time-dependent-DFT method with the CAM-B3LYP functional (33).

2.2.5 CAM-B3LYP

CAM-B3LYP is a new hybrid exchange–correlation functional with improved long-range properties. It is the combination of the hybrid qualities of B3LYP, and the long-range correction presented by Tawada et al(37, 38). The hybrid functional B3LYP is the most widely used function in DFT but it has weaknesses which are covered by CAM-B3LYP. CAM-B3LYP was found to be superior with regards to:

- Accurate calculation of long chains polarizabilities(39)
- Calculating excitation energies with the TD-DFT method (40)
- Predicting molecular charge-transfer spectra (41)

2.2.6 Time-Dependent Density Functional Theory (TD-DFT)

Time-dependent Density Functional Theory (TD-DFT) explores the dynamic behavior of electronic systems over time, enabling the study of processes like electronic excitations and responses to external forces. The description of TD-DFT and linear response description below is adapted from the book ‘Principles and Applications of Quantum Chemistry’ by Gupta (34).
The electron density that comes out of the time dependent DFT calculations frequently oscillates between the ground and the first excited states. From this solution, it is possible to extract both these states. Time-Dependent Density Functional Theory (TD-DFT), proposed by Runge and Gross (RG theorem) in 1984, is probably the most widely used theoretical approach to compute the transition energies, vertical and adiabatic excitation energies. For dynamic electronic processes

like photoelectron spectroscopy, this approach is also useful. TD-DFT is indeed an extension of DFT with a similar computational foundation. The TD-DFT method relies on features of the ground state and the corresponding energies of its orbitals. Consequently, the excited state energy is calculated with the properties of the ground state. The R-G theorem is derived from the HK theorem for the time-dependent Schrödinger equation. It indicates that, for many-body systems evolving from a given initial state, there is a one-to-one correlation between the external (time-dependent) potential, $V_{ext}(r,t)$, and the electron density, ρ (r,t) . In the R-G theorem, the expectation value of any physical observable in the ground state of a many-electron system is a unique functional of the time-dependent electron density ρ(r,t) and of the initial state Φ^0 corresponding to time: t=0, $\Phi^0 = \Phi(t=0)$ (34).

The Kohn and Sham (KS) method avoids solving the interacting Schrödinger equation for the electrons' wavefunction by, instead, determining the electron density; in TD-DFT, the same approach is used. TD-DFT uses the non-interacting particles method that is controlled by an external local potential $V_{KS}(\rho,t)$ unique to the non-interacting system. The density of noninteracting electrons is the same as the density ρ(r,t) of the original interacting system. In the time-dependent case, these KS electrons obey the time-dependent Schrödinger equation(34):

$$i\frac{\partial}{\partial t}\phi_i(r,t) = \left[-\frac{\nabla^2}{2} + V_{ks}(r,t)\right]\phi_i(r,t) \qquad 5$$

Time-dependent KS orbitals can be used to determine the electron density of the interacting system(34):

$$\rho(r,t) = \sum_{i}^{occ} \left|\phi_i(r,t)\right|^2 \qquad 6$$

Eq.5, which includes a single practical equation, is quite simple to solve numerically. If the precise KS potential is given, V_{KS}, Eq.6 could be used to get the exact KS orbitals and, from these, the density of the system. The KS potential is conventionally separated in the following way(34):

$$V_{ks}(r,t) = V_{ext}(r,t) + V_H(r,t) + V_{xc}(r,t) \qquad 7$$

Here, the first term is external potential (such as the potential from the nuclei) and the second is the Hartree potential which explains the classical electrostatic interaction between the electrons.

The last term is the exchange-correlation (*XC*) potential, which includes all the nontrivial many-body effects (34).

A TD-DFT calculation proceeds as follows: Initially, a set of N orthonormal Kohn-Sham (KS) orbitals (Φ_i) is selected. These orbitals must accurately represent the exact density of the true initial state Ψ_0, as well as its first time-derivative. The time-dependent KS equation (Eq. 5) is then utilized to evolve these initial orbitals, accounting for the external potential, the Hartree potential, and an approximate description of the exchange-correlation (XC) potential (Eq. 7). In most TD-DFT applications, the adiabatic approximation is employed, ie. the XC potential responds instantaneously and without memory responds to any changes in the charge density over time(34).

In a TD-DFT calculation, it is possible to bypass the complicated time-dependent Kohn-Sham (KS) equation if the external potential is weak. Instead, the linear response theory (LR) can be employed assuming that the correction term due to excited state interactions are small. This is the case in the present study when we determine the absorption and fluorescence excitation spectra of a molecule due to interaction with weak electromagnetic radiation (34).

2.2.7 Linear Response approach

When the external time-dependent potential is small, solving the full-time-dependent KS equation may not be necessary. In such cases, perturbation theory can provide an appropriate replacement for explaining the behaviour of the system. According to perturbation theory, a problem's exact solution can be used to approximately solve a related, simpler problem. When the differences between the approximate and true wave functions are small, it is helpful because the system is barely affected by the omitted terms. According to the HK theorem for the ground state, the external potentials can be uniquely determined from the electron density. By solving the many-body Schrödinger equation using the external potential, we can obtain the energies of the system. Similarly, the excitation energies of the system can also be viewed in terms of the ground state density, as they are functional derivatives of it. However, expressing observables and excitation energies in terms of the ground state density is often challenging, because limited information is available in this regard. One solution is to use linear-response TD-DFT theory to solve this problem. This method has benefits because it allows for the use of all the features of DFT, as the system's

response depends on the ground state wavefunction. Assume that a system is initially in its ground state, with nuclear potential v_0 and electron density ρ_0. When it undergoes a perturbation $v^{(1)}$, the total external potential will be $V_{ext}(t) = v_0 + v^{(1)}$ and the electron density of the system will change to $\rho(r,t)$ such that (34):

$$\rho(r,t) = \rho_0(r,t) + \rho^{(1)}(r,t) + \rho^{(2)}(r,t) + \ldots \quad 8$$

If the time-dependent external potential is small, we can restrict ourselves to the first-order of perturbation in the density, $\rho^{(1)}$. Since the density of the noninteracting system in the KS formalism is used to calculate the density of the interacting system of electrons, we can write(34):

$$\rho^{(1)}(r,\omega) = \int \chi_{KS}(r,r',\omega)\upsilon_{KS}^{(1)}(r',\omega) \quad 9$$

where the potential $\upsilon_{KS}^{(1)}$ entering this equation is just a linear change of υ_{ks} and similar to Eq.9 and χ is called the density-density response function. It is the density of density functional theory and is the basic quantity in the LR-TD-DFT which relates the first-order density response to the applied perturbation. It is much simpler to calculate χ_{KS} than χ because it is the density response function of the system of particles that are not interacting. The true density response (χ) can be determined from the KS system by using a Dyson-like equation. Then it is possible to calculate excitation energies with this value(34).

2.2.8 Solvent role in the computational calculation

In DFT and HF theory which were discussed above, all functions are for non-interacting molecules in the gas phase without any external potential and interaction. Ab *initio* technique may also be used to determine the properties of a (solute) molecule when it is surrounded by other molecules (solvent). Solvent-solute interactions may have to be calculated explicitly when accurate energies are required, or when strong binary interaction dominate, such as H-bond. At the other end of the complexity scale, one may simply approximate the solvent interactions with the solute as those of an unstructured and homogenous dielectric continuum. In that case only the dielectric constant of the solvent is required and the shape of the cavity, which is occupied with the solute molecule, where that shape is sometimes approximated to be a sphere or ellipsoid. The polarized continuum model (PCM) is a simple compromise solution; it defines the solute cavity as a function of the

electron density of the solute in the actual shape of the molecule. It also allows the solvent continuum to be polarized and provides a good approximation of solvent-solute interaction energies as long as those are mostly electrostatic in nature (42).

2.2.9 Nonequilibrium and equilibrium calculations

There is a distinction between equilibrium and non-equilibrium calculations for phenomena related to sudden changes in the charge distribution in the solute molecule following the solute's electronic transition to an excited state.

The effect of the solute electronic charge distribution on the solvent environment can be discussed in terms of the electronic and orientational polarizations of the solvent. Following a rapid change in the solute's dipole moment, the electron distribution in the solvent molecules changes in a rapid process (governed by the solvent's polarizability), but the solvent molecules can also reorient themselves in a much slower process in response to solute dipole moment changes ("orientation polarization").

Consequently, the solvent's response to changes in the solute's dipole moment can be determined computationally in two separate calculations:

- An "equilibrium calculation" for a situation in which the solvent had enough time to react to a rapid change in the solute's charge distribution. This amounts to an *ab initio* geometry optimization.
- A "non-equilibrium calculation" to capture processes which are too rapid for the solvent orientation to fully respond to. The fast part of the solvent response i.e., the electronic redistribution can follow such a dynamic process while the remaining degrees of freedom (nuclei) remain unchanged and in the initial state. This model corresponds to the Franck-Condon approximation, leading to a "vertical" electronic excitation process. Two different approaches have been developed for describing nonequilibrium solvent effects: the linear response (LR) approach and the state-specific (SS) approach (43).

Below we focus on the corrected linear response approach, the method used in our study.

2.2.10 Corrected linear response approach

Based on the research of B. Mennuicci and J. Tomasi et al. on solvent role in the computational calculation of the solute's excited state, two formalisms exist to compute excited state energies with polarizable solvation models: state-specific (SS) and linear-response (LR) (43, 44).

The SS and LR techniques give different answers in calculating excited state energies for molecules in the presence of a solvent.

The nonlinear Schrödinger's equation for the ground and excited states is resolved in state-specific theory. This method assumes that the excitation energy is the difference between the free energy of the excited state and the free energy of the ground state (43).

$$\Delta G_{0i} = G_i^{neq} - G_0 \qquad 10$$

Here, G_i^{neq} is the free energy of the ith excited state in a non-equilibrium calculation. Non-equilibrium implies that upon a vertical excitation in this system, the slow degrees of freedom of the solvent (nuclei) remain equilibrated with the solute wave function in its ground state $|0\rangle$, while fast degrees of freedom of solvent (i.e. solvent electrons) are in equilibrium with the solvent nuclei (slow components) and the solute wave function in the excited state $|i\rangle$. In other words, the solvent molecules' polarizability is explicitly included in its response to the difference solute molecule's charge distribution in the solute excited state. The non-equilibrium excitation energy corrected to the first state based on Eq.10 is obtained (43, 44):

$$\Delta G_{0i}^{ss} = \Delta E_{0i}^{0} + \frac{1}{2}\left[\left\langle i^0 \middle| \hat{V} \middle| i^0 \right\rangle - \left\langle 0 \middle| \hat{V} \middle| 0 \right\rangle\right].\left[\left\langle i^0 \middle| \hat{Q}_d \middle| i^0 \right\rangle - \left\langle 0 \middle| \hat{Q}_d \middle| 0 \right\rangle\right] = \Delta E_{0i}^{0} + R_{dyn}^{ss}(P_{0i}^{\Delta}) \qquad 11$$

where ΔE_{0i}^{0} is the zero-order excitation energy which corresponds to the transfer of one electron from the ground state to an excited state when the fixed reaction field of the ground state, V_0, is present. $|i^0\rangle$ is the i-th electronic state obtained in the presence of the fixed reaction field due to the ground state $|0\rangle$. In the PCM solvent model, $\hat{V}$ is the molecular electrostatic potential operator. $\hat{Q}$ is the "apparent charge operator" an operator that is affected by the partition of the surface, the solvent permittivity and the size and shape of the cavity all affect it. $\hat{Q}$ represents the polarization of the solvent under the electrostatic potential created by the solute in terms of apparent surface distribution which spreads on the surface of the cavity containing the solute

molecule. The operators $\hat{Q}$ and $\hat{V}$ form together a nonlinear operator that describes the solvent polarization in the presence of the solute nuclei and electrons is called the electrostatic interaction operator. $V(\psi_i)$ is divided into an inertial part $V_{in}(0)$ and dynamic part $V_d(i)$. In this way, $\widehat{Q_d}$ can be understood as the apparent charge operator for only the dynamic response of the solvent, while the inertial part is included in ΔE_{0i}^0 (43).

By contrast, in the LR model, the excitation energies are defined as the frequency-dependent linear response functions of the molecular system in the presence of solvent in the ground state, avoiding explicit calculation of the excited state wave function (43, 44).

$$\Delta G_{0j}^{LR} = \Delta E_{0j}^{0} + \left\langle j^0 \left| \hat{V} \right| 0 \right\rangle . \left\langle 0 \left| \hat{Q}_d \right| j^0 \right\rangle = \Delta E_{0j}^{0} + R_{dyn}^{LR}(P_{0j}^{T}) \qquad 12$$

The first term of the equation, ΔE_{0j}^0, is as same as the first term of Eq.11. The second term corresponds to the energy of the interaction between the reaction field brought on by the transition density and the transition density.

Overall, in the LR approach, the response of the solvent dynamic polarization to the excitation, R_{dyn}^{LR} , is computed from the transition density, P_{0j}^{T}, while in the SS approach, the R_{dyn}^{ss} is determined by the difference of the electron densities of the ground and excited states, P_{0i}^{Δ} (44).

The LR formulation is particularly effective for transitions that involve small changes in electron density because the electrostatic interaction between the solvent and the excited state density is similar to the ground state. In contrast, for the excitations with significant rearrangements in the density, the LR scheme falls short because it fails to consider the density-dependent relaxation of the solvent polarization. For this reason, the LR approach is modified by including a state-specific (SS) correction term to calculate the excitation energy of solute in the solvent with a single calculation in an approach which is called the corrected linear response approach (cLR). As previously mentioned, the free energy of the ground state can be used to calculate the equilibrium and non-equilibrium excited states. The solvent reaction field has plenty of time in the equilibrium model to relax from the initial ground state value to the excited state value, which represents the new solute-solvent equilibrium. The combination of the energy of the dynamic solvent that is in equilibration with the excited solute and the inertial solvent that is frozen in the ground state

makes up the excited state energy in the nonequilibrium. As a result, the excited state can be determined by calculating the frozen PCM energy, E_0^i, and the relaxation term of the density matrix, P_Δ^{neq}.

In the cLR approach, the vertical transition energy to the excited state is equal to the Eq.10 but G_i^{neq} becomes (43):

$$G_i^{neq} = G_0 + \omega_i^0 + \frac{1}{2}\sum_i v(s_i; P_\Delta^{neq}) q_\Delta^{dyn}(s_i; P_\Delta^{neq}) \qquad 13$$

Where $\omega_i^0 = \Delta E_0^{i0} = E_0^i - E^0$ is the difference of the excited state energy and ground state energy in presence of a PCM reaction field that is kept frozen in the ground state geometry.

$V(\psi_i)$ is defined as the electrostatic interaction between an apparent charge density on the cavity surface, as was previously mentioned. In a paper on cLR formalism, the boundary-element method (BEM) is used which is a computational technique that divides the cavity surface into *its* discrete elements, known as *tesserae*, and replaces the apparent surface charge density with a group of point charges q_i that are positioned at the centre of each *tessera*. Therefore the $\hat{V}_i$ indicates the electrostatic potential operator computed on the surface element s_i and $V(s_i)$ the corresponding expectation value.

In the cLR approach, the relaxation part of the density matrix, P_Δ^{neq}, and the corresponding apparent charges, q_Δ^{dyn}, are determined with the extension of the TD-DFT approach. Then, the excited state energy is calculated with Eq.13 , which covers the LR approach limitation.

All the above equations and their description are obtained from two articles from B. Mennuicci and J. Tomasi et al. who are the creator of this approach. In Eq.13, all the *K* subscripts of the paper are exchanged with *i* to maintain the connection with the rest of the equations (43).

2.3 Description of molecular and solvent properties

In this section, several concepts and equations are introduced that will serve us to understand the physical processes described in chapters 3 and 4. Most of them are well-understood and can even be found in textbooks, but our study brings these concepts together in, sometimes, unconventional ways.

2.3.1 Twisted Intramolecular Charge Transfer

Intramolecular electron transfer processes are a common and important phenomenon that frequently occurs upon photoexcitation of an absorbing compound. These processes have in common that a charge separation or transfer happens upon excitation, i.e. the dipole moment of the molecule in its excited state is very much different (usually larger) than in the ground state. Molecules and inorganic metal-ligand complexes can be designed to exhibit electron transfer. Since the transition dipole moment is related to the electron distribution in ground and excited states (discussed below) these transitions tend to be bright and lead to prominent absorption features. Organic molecules, including many dyes, can be designed to exhibit intramolecular electron transfer upon excitation to their first excited state. These molecules have an electron donor moiety and an acceptor moiety which may be connected either by single bond(s) or by a π-conjugated system. It has been recently realized that the charge separation can be further enhanced and made longer-lived, if the molecule in its excited state changes its configuration so that the π-conjugation is broken, and the donor and acceptor moiety are no longer resonantly coupled (11). These so-called Twisted Intramolecular Charge Transfer (TICT) states have found a variety of interesting applications in molecular electronics, chemo-sensing, and bioimaging (8, 9). Donor-acceptor organic compounds having TICT states sometimes show “dual fluorescence”, i.e. they show fluorescence at two different wavelengths, each having a different fluorescence lifetime, as well as solvatochromic and fluorogenic responses. Dual fluorescence in the TICT model is caused by a radiationless energy redistribution which causes dihedral angle changes between donor and acceptor groups leading to a twisted charge transfer state. If the locally excited state has a lifetime that can compete with this fast-twisting motion, the TICT state and the locally excited (LE) state can exist in equilibrium, and one can observe fluorescence from both minima in the excited states, i.e. from two different excited-state conformers which may have quite different charge distributions (45).

The formation of the TICT state depends on the balance of two interacting forces. Since a conjugated π-system prefers a coplanar conformation, synthetic chemists add functional groups which introduce steric hindrance to coplanarity. Steric bulk is the term used to describe the spatial hindrance or crowding around a molecule caused by large substituents or groups in the context of molecular interactions and electronic transitions. The dynamics and characteristics of molecules, including their excited states and transitions, can be influenced by steric effects. Steric interactions

twist the D-A junction and promote the charge transfer (CT) state, while π-conjugation drives a coplanar arrangement and stabilizes the local excited state (LE) (Figure 8-d) (13).

These two conformations in the excited state usually have a very different dipole moment. While the CT state has a large dipole along the donor-acceptor axis, the dipole of the LE state is typically far smaller and may not be aligned along the donor-acceptor axis(13).

A molecule with a large dipole moment is stabilized in a polar solvent environment. Excitation energies have therefore been used to differentiate between CT states and LE states, where emission from CT states is expected to show strong solvatochromic shifts due to the stabilization of the dipolar excited state compared to the ground state (13).

Synthetic chemists control the relative stability of the LE and CT states by modifying the molecular structure, where the identity of the donor and acceptor groups, and their conjugation across either single bonds or a linker group, are the most obvious modifications. By modifying the steric restrictions, it is simple to manipulate the competition between the LE and ET characters of CT. The CT surface is deformed by some steric hindrances, resulting in a severely twisted conformation where the minima are located. The CT minimum in this conformation becomes a highly twisted and polarized state (i.e., TICT state) because the LE state is too destabilized to mix with the ET state effectively (Figure 8-c). On the other hand, the LE state is sufficiently stabilized when a steric restriction, like a carbon bridge between a donor and an acceptor, forces the D-A junction to be coplanar, resulting in the CT minimum being governed by LE character (i.e. coplanar ICT state - Figure 8-d) (13).

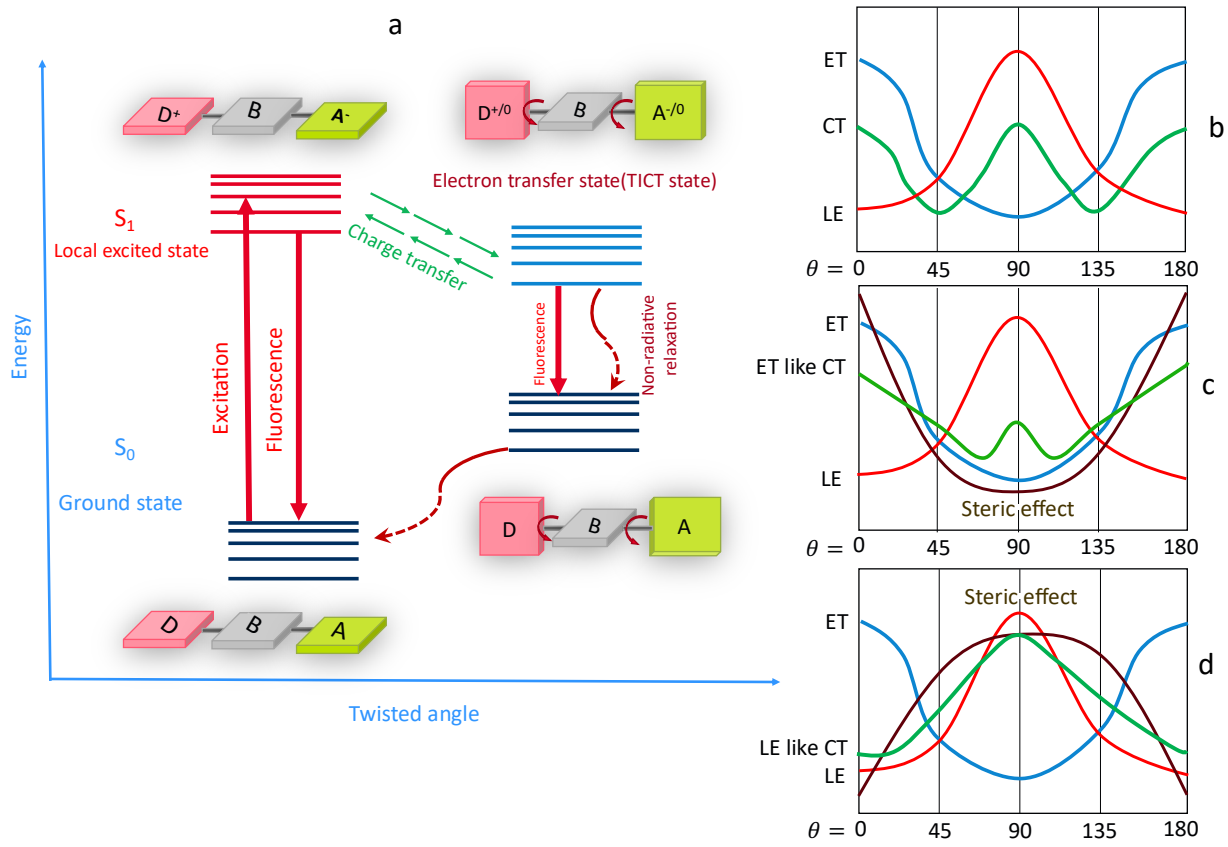

Figure 8 (a) Twisted intermolecular charge transfer dynamic (b) LE and ET energy states on an adiabatic energy surface of CT (c) the altered energy diagram when the steric restriction is introduced to twist the D–A junction (d) the altered energy diagram when the D–A junction is made coplanar (13)

There are many degrees of freedom in a donor-acceptor dye, but those that are most meaningful in characterizing the excited state surface are the dihedral angles, θ, between the donor and acceptor groups, or, if the molecule contains a linker the two dihedral angles between donor/linker and linker/acceptor. The dihedral angles signify conjugation and steric hindrance. If the dihedral angle in the excited state is much larger than that of the ground state, we can presume that a TICT state has been formed. If both minima are energetically accessible and the barrier between them is small, we can use the Arrhenius equation to explain the transition rates, K_a and K_b, and the equilibrium distribution between the population in the locally excited state, LE, and the TICT state. In Figure 9, The relation between transition rates and the nonradiative decay rate is shown based on a review article 'Quantitative Design of Bright Fluorophores and AIEgens by the Accurate Prediction of Twisted Intramolecular Charge Transfer (TICT)' (46). Also, the quantum yield dependency on the nonradiative decay rate is given.

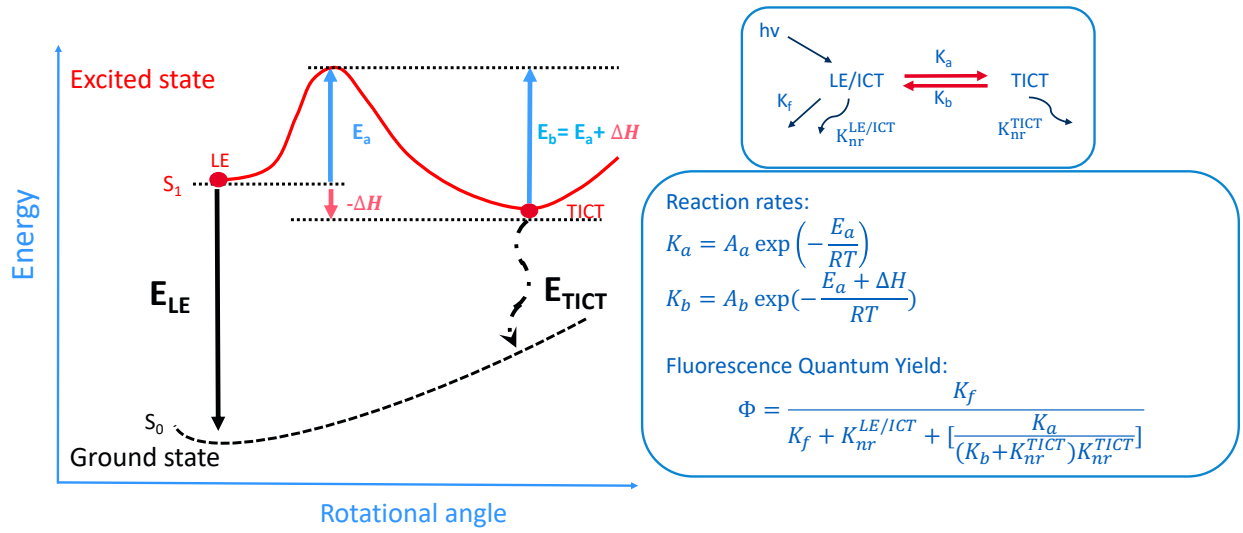

Figure 9 Experimental approach to of the LE to TICT state photoreaction corresponding calculations of reaction rates and fluorescence quantum yield using Arrhenius equation K_f and K_{nr} are radiative and non-radiactive rates, respectively (46).

The rotation barrier (E_{RB}) and driving energy (E_{DE}) are required for evaluating the possibility of occupying the TICT state. In Figure 9 they correspond to the activation energy E_a and to the total change in enthalpy ΔH of the reaction respectively. The dependency of energy and rotational angle that relate these two properties to the TICT state are shown in Figure 10. TICT formation cannot spontaneously occur with positive E_{DE} (Figure 10-a), i.e. the TICT state has to be energetically stabilized compared to the LE state. When $E_{RB} > 0$ and $E_{DE} < 0$, both LE and TICT states are populated (Figure 10,b). As E_{RB} approaches 0, the TICT state will more easily form. Depending on the non-radiative decay constants of the two states, K_{LE} and K_{TICT}, the quantum yield, Φ, changes with the population of the TICT state. The quantum yield is typically significantly lower for TICT state fluorescence compared to fluorescence emission from the LE state (Figure 10,c)(46).

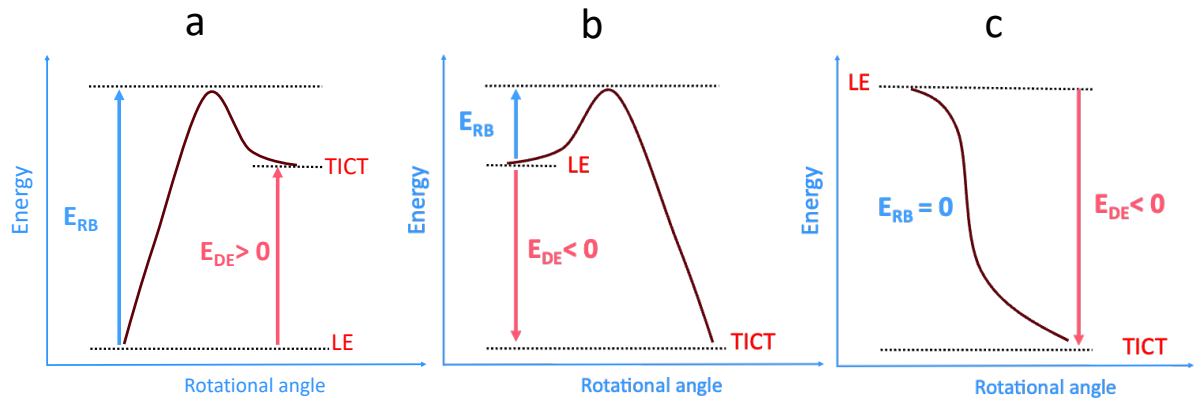

Figure 10 Theoretical model of excited states, LE to TICT state, photoreaction

2.3.2 Polarity, Dipole moment, Polarizability and Polarization

Solvent polarity is a somewhat ill-defined concept that describes how different solvents can stabilize charged (or dipolar) solutes. Different definitions for polarity are in use, today, with some based on the solvent's dielectric constant and others on empirical scales based on solvatochromic shifts observed with for example Reichardt's dye, E_T(30), or Nile Red, E_T(33). Reichardt's dye is an azomerocyanine betaine class organic dye. This dye's solvatochromic characteristics make it notable. The solvent molecules' dipole moment usually plays a large role in its polarity, but its relative size also matters. For example, water (μ = 1.85 D; ε_r = 80) has a very large polarity of E_T (30) = 63, whereas the larger acetone molecule (μ = 2.88 D; ε_r =21) has a lower polarity of E_T(30) = 42 (47).

The dipole moment measures the charge separation in a molecule. All polar molecules have a net dipole moment due to their unequal electron distribution. The dipole moment of a molecule is calculated using the equation (22):

$$\mu = \sum q.r \qquad 14$$

μ is the dipole moment, q is the magnitude of charge, and r is the distance between the two charges that are separated of the charge. Here, μ and r are vectors, which are quantities having a direction as well as a magnitude. Charge separation results a dipole moment. In the ground state

of molecules dipole moments can be used to determine electronegativity differences between two atoms.

Polarizability, α, is the measure of the tendency of matter to acquire an induced (non-permanent) electric dipole moment, μ, as a response to an applied electric field, ε. This phenomenon is a property of all matter when we consider that matter is built up of elementary particles having an electric charge, that is protons and electrons. A common approach to determine the polarizability of a molecule is through time-independent perturbation theory.

Eq.15 expresses the energy in powers of perturbation. Shown, here, is the first order perturbation to the Hamiltonian, representing the change in the Hamiltonian due to the presence of the external electric field, ε, where H^1 is the first degree of the Hamiltonian (22):

$$H^1 = -\mu.\varepsilon \qquad 15$$

With Eq.15 we can drive the polarizability from the perturbation expression for the energy. The key to the extraction of the polarizability from the perturbation expression for the energy is the Hellmann-Feynman theorem. The Hellmann-Feynman theorem presents in Eq.16 which consider a system characterized by a Hamiltonian that depends on a parameter P. This parameter must be the internuclear distance in a molecule or the strength of the electric field to which the molecule is exposed(22):

$$\frac{dE}{dP} = \left\langle \frac{\partial H}{\partial P} \right\rangle \qquad 16$$

In the present case to extract polarizability, the parameter *P* is the electric field, ε (22):

$$\frac{dE}{d\varepsilon} = \left\langle \frac{\partial H}{\partial \varepsilon} \right\rangle \qquad 17$$

The partial derivatives of the Hamiltonian operator are expressed as Eq.18(22):

$$\frac{\partial H}{\partial \varepsilon} = \frac{\partial H^{(0)}}{\partial \varepsilon} + \frac{\partial H^{(1)}}{\partial \varepsilon} = \frac{\partial H^{(1)}}{\partial \varepsilon} = \frac{\partial}{\partial \varepsilon}(-\mu_z \varepsilon) = -\mu_z \qquad 18$$

because for the zero-order Hamiltonian, H^0, there is no electric field.

It follows that the change of energy with the electric field is mentioned in Eq.19(22):

$$\frac{dE}{d\varepsilon} = -\langle \mu_z \rangle \tag{19}$$

Using a Taylor expansion, the energy of a molecule in the electric field given by(22):

$$E = E_{(0)} + \left(\frac{dE}{d\varepsilon}\right)_0 \varepsilon + \frac{1}{2!}\left(\frac{d^2E}{d\varepsilon^2}\right)_0 \varepsilon^2 + \frac{1}{3!}\left(\frac{d^3E}{d\varepsilon^3}\right)_0 \varepsilon^3 + \ldots \tag{20}$$

where $E_{(0)}$ is the energy of the system in the absence of the electric field and subscript 0 means the derivative is determined at $\varepsilon = 0$. The combination of Eq.19 and 20 provide a Taylor expansion of the expectation value of the dipole moment(22):

$$\langle \mu_z \rangle = -\left(\frac{dE}{d\varepsilon}\right)_0 - \left(\frac{d^2E}{d\varepsilon^2}\right)_0 \varepsilon - \frac{1}{2}\left(\frac{d^3E}{d\varepsilon^3}\right)_0 \varepsilon^2 - \ldots \tag{21}$$

The electric dipole moment value of a molecule in the presence of an electric field is therefore equal to the sum of a permanent dipole moment, μ_{0z}, and the dipole moments induced by the electric field(22):

$$\langle \mu_z \rangle = \mu_{0z} + \alpha_{zz}\varepsilon + \frac{1}{2}\beta_{zzz}\varepsilon^2 - \ldots \tag{22}$$

Here α_{zz} is the polarizability and β_{zzz} is the hyperpolarizability both in the z-direction. The polarizability indicates the linear relationship between the molecular dipole moment and the applied electric field, whereas the hyperpolarizability refers to the higher-order coefficients that characterize the non-linear response of the molecular dipole moment. Finally, the relation between the energy of the system, E, and polarizability, α_{zz}, in the presence of an applied electric field, ε, is readily determined from (20) and (22) (22):

$$E = E_{(0)} - \mu_{0z}\varepsilon - \frac{1}{2}\alpha_{zz}\varepsilon^2 - \frac{1}{6}\beta_{zzz}\varepsilon^3 + \ldots \tag{23}$$

By the existence of the induced surface charge density, polarization is also the dipole-moment density of the medium. Dipole moment density is the mean dipole moment of each molecule in the medium, multiplied by the density of molecules, $\mathcal{N} = N/V$. Nonpolar solvent molecules do not have a permanent dipole moment and $\langle \mu \rangle$ is the induced dipole moment. The molecules experience the local electric field,ε^*, the solvent polarization can be written as (22):

$$P = \alpha \mathcal{N} \varepsilon^* \qquad 24$$

Polar solvent molecules have a permanent dipole moment in addition to the induced dipole moment, so the total polarization of a medium included polarizable ($\alpha > 0$) polar molecules (μ >0) is given by the Clausius-Mosotti equation:

$$P = \left(\alpha + \frac{\mu_0^2}{3KT} \right) \mathcal{N} \varepsilon^* \qquad 25$$

Eq.25 shows the dependence of polarization on polarizability and permanent dipole moment (22).

2.3.3 Orientation polarization - Relative permittivity – Refractive index of medium

When the polarizability of a molecule is discussed, the properties of dielectric media around the molecule have an important role. These properties include relative permittivity and refractive index. The relative permittivity, ε_r,is the ratio of the permittivity of a material, ε, to the electric permittivity of the vacuum, ε_0. The relative permittivity is (22):

$$\varepsilon_r = \frac{\varepsilon}{\varepsilon_0} \qquad 26$$

Previously, the relative permittivity was called the dielectric constant. The relative permittivity can be understood as the ability of an insulator (a “dielectric”) to store electric energy in an electrical field, or equivalently the capacitance of a capacitor having the material as a dielectric compared to a capacitor having vacuum between the capacitor plates. The relative permittivity is large for media that exhibit large polarization, i.e. that either have a large orientation polarization (requiring a dipole and compact size), *or* that have large electronic polarizability, i.e. by having π-conjugated systems, or large atoms, or those that have both large orientation polarizability and large electronic polarizability. The refractive index, n , is the ratio of the speed of light in a vacuum to its

speed in a medium. If the relative permittivity can be understood to the response of a medium to a very slow change of electric field, the refractive index is a measure for the polarization response of a medium to an electromagnetic field that changes at approximately 10^{14} Hz. At these high frequencies only electronic polarization matters, and only those molecules and atoms with high electronic polarizability also exhibit high refractive index. Comparing the refractive index of benzene (n_D = 1.501) with that of cyclohexane (n_D = 1.426) the influence of the π-system is apparent.

The shift in the emission spectra of a molecule can be attributed to the interaction between the molecule and the surrounding solvent. This interaction affects the energies of the ground and excited states of molecule. The primary factor responsible for this shift is the polarity of the solvent. The separation of charge within the solvent molecules determines a solvent's polarity. Because the distribution of charge within the molecule is unbalanced, polar solvents have a permanent electric dipole moment, resulting in a positive and negative end. Nonpolar solvents have a relatively uniform charge distribution and, as a result, a minor permanent dipole moment. Polarizability is a measure of how easily an external electric field can distort the electron distribution within a molecule. The greater a molecule's polarizability, the more it can be polarised by an external electric field. In the context of a solvent-solute interaction, a more polarizable solvent can be more easily polarised by the charge distribution of the solute. When a molecule is immersed in a polar solvent, the permanent dipole of the solvent interacts with the solute, the energy of electronic transitions like absorption or emission causing a shift in the energy levels of the molecule's ground and excited states.

Furthermore, the solvent's polarizability, or ability to be polarised, influences the extent to which the solvent molecules can be distorted by the solute's charge distribution. A highly polarizable solvent will respond to the solute more readily, resulting in a larger energy shift in the spectra.

Orientation polarization,Δf, depends on the relative permittivity and refractive index of the solvent (22).

The meaning of orientation polarization is described here by a simple example: when an external electronic field (like a solvent around the solute) is applied to a molecule like water (solute) that has a permanent dipole moment, the orientation of the permanent dipole would be changed, this process is called the orientation polarization, Δf(16).

$$\Delta f = \left(\frac{\varepsilon_r - 1}{2\varepsilon_r + 1}\right) - \left(\frac{n^2 - 1}{2n^2 + 1}\right) \quad 27$$

The spectral shifts resulting from the redistribution of electrons in the solvent molecules and the reorientation of solvent dipoles are explained by the first term ($\frac{\varepsilon_r - 1}{2\varepsilon_r + 1}$). Only the redistribution of electrons is considered by the second term ($\frac{n^2 - 1}{2n^2 + 1}$). The term orientation polarizability is explained by the difference between these two terms, which also accounts for the spectral shifts caused by the solvent molecules' reorientation(16).

2.3.4 Transition dipole moment

The transition dipole moment is a vector that describes the dipole associated with an electronic transition between an initial state, and a final state (i $\rightarrow$ f) of a molecule.

$$\mu_{fi} = \int \psi_f^* \hat{\mu} \ \psi_i d\tau \quad 28$$

where the $\hat{\mu} = e\hat{r}$ is the electric dipole moment operator. To determine whether transitions are permitted by electric dipole interaction, one determines the transition dipole moment. If the integral describing the transition dipole moment (28) is nonzero, the transition between the initial state, ψ_i, given by wavefunction and the final state, ψ_f, is allowed. Transition can be forbidden if they require a change in multiplicity (electronic spin), or if the symmetry of the involved orbital force the integral in to be close to zero.

In a one-electron transition the initial and final molecular orbitals involved in the electronic transition determine the magnitude and the direction of the transition dipole moment (48).

2.3.5 Oscillator strength

Three main factors affect a spectral band's intensity. These are the oscillator strength, f, the concentration of the absorbing species, and the length of the light path through the sample. An estimate of the probability of electronic transition electron between two states can be calculated by using the dimensionless spectroscopic term known as oscillator strength. It quantifies the strength of the absorption or emission of light associated with that transition.

$$f_{fi} = \frac{8\pi^2 m_e \nu \left|\boldsymbol{\mu}_{fi}\right|^2}{3he^2} \qquad 29$$

Where m is the mass of an electron, *h* is the Planck constant, μ_{fi} is transition dipole moment, ν is the frequency of absorbed light and *e* is the charge of the electron. The oscillator strength is unity for an electron that is allowed to oscillate harmonically in three dimensions, i.e. with its wavefunctions given by a simple harmonic oscillator. For fully allowed transitions the experimentally observed oscillator strengths are approaching unity, whereas for spin-forbidden transition the oscillator strengths tend to be below 10%.

Interestingly, the molecule's polarizability can be expressed in terms of the experimentally obtained oscillator strengths.

$$\alpha = \frac{\hbar^2 e^2}{m_e} \sum{}' \frac{f_{fi}}{\Delta E_{fi}^2} \qquad 30$$

where ΔE_{fi} is the energy difference between the electronic states n and 0. In a spectrum the oscillator strength of transition of a molecule is determined by the band intensities and the energy of a molecule is determined with bands location on frequency scale. Equation 30 shows that molecules having intense colour also tend to be polarizable (22).

Chapter 3

3.1 Experimental

3.1.1 Carbazole–bromobenzothiadiazole (CBB)

The organic orange-colored carbazole-bromobenzothiadiazole (CBB) was synthesized and described in some detail by Chernick et al. previously, and we outline only a few of its features here (1). CBB is composed of three functional groups: a carbazole (CBz) donor moiety and a bromine-substituted benzothiadiazole (BTD) acceptor moiety are connected through a phenylthiophene (PT) bridge to form the compound shown in Figure 11. Three dihedral angles that connect the functional groups are created by the extended bridge, which take on a twisted configuration in the crystalline state, as X-ray diffraction shows (1). A relatively long phenylthiophene (PT) bridge was chosen to prevent the lowest unoccupied molecular orbital (LUMO) and the highest occupied molecular orbital (HOMO) from overlapping. In addition, a large electronic dipole moment is expected in the excited state considering that the charge separation occurs over a very large distance between donor and acceptor group (1). With this study we examine how CBB behaves when its environment is altered using experimental data supported by calculations. By varying the polarity and the viscosity of the CBB environment and obtaining its excitation-emission matrix (EEM) spectra, we can assess its behaviour. From these spectroscopic properties, CBB energies and dipole moments in different states are calculated using a solvent model in order to compare computational findings to those from experiments.

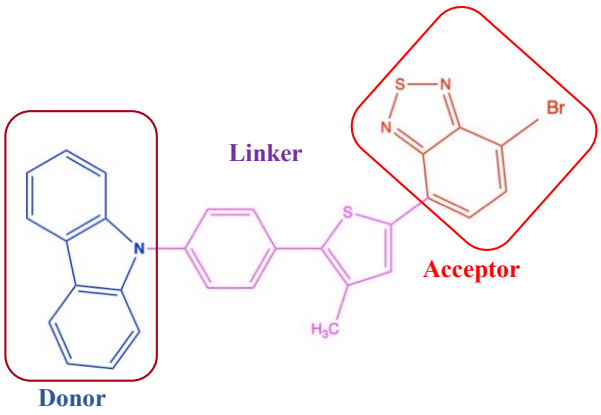

Figure 11 Carbazole–bromobenzothiadiazole molecular structure (top) orange powder (below)

3.1.2 Viscosity effect

To show the influence of viscosity on the CBB fluorescence spectra, two different types of solvents are used in an experiment. Group one includes toluene and chloroform which have nearly the same viscosity and different orientation polarization. Group two includes polyethylene glycol (PEG400) and 1,2dichlorethane with nearly the same orientation polarization and a different viscosity (**Table 1**). All the solution concentrations are 25.54 ppm by mass.

	Viscosity, η at 25 °C [m.Pa.s]	Relative permittivity, ε_r at 20 °C	Refractive index, n at 20 °C	Orientation polarization, Δf	V_{ss} [cm^{-1}]
Acetonitrile	0.369	36.64	1.3442 (30^0C)	0.305	6974
Cyclohexane	0.894	2.024	1.4235 (25^0C)	0.000	3899
Acetone	0.306	21.01	1.3588	0.284	6828
Toluene	0.560	2.379	1.4941	0.012	5170
Chloroform	0.537	4.807	1.4459	0.148	5556
1,2-dichloroethane	0.779	10.42	1.4422	0.222	5997
PEG400	92.797(49)	11.42(50)	1.4650 (49, 51)	0.221	6122

Table 1 *Solvents properties(52) The last column is the stokes shift of CBB in different solvents which are obtained by Varian Carry Eclipse*

Figure 12 (top) Freshly prepared solution of CBB dissolved in acetonitrile – acetone – chloroform – toluene – cyclohexane from left to right (below) Peg400

Four EEM spectra from the Varian Carry Eclipse spectrometer are shown in Figure 13. Two excited states result in a fluorescence peak in all of the EEM spectra. In the first solvent group (toluene

and chloroform), changing the orientation polarization of the environment causes an almost 50 nm shift in the emission spectra, but in the second group (PEG400 and 1,2 Dichloroethane) changing the viscosity has no effect.

Dichloroethane	PEG400
Similar Dielectric constant, Different Viscosity	

Chloroform	Toluene
Different Dielectric constant , Similar Viscosity	

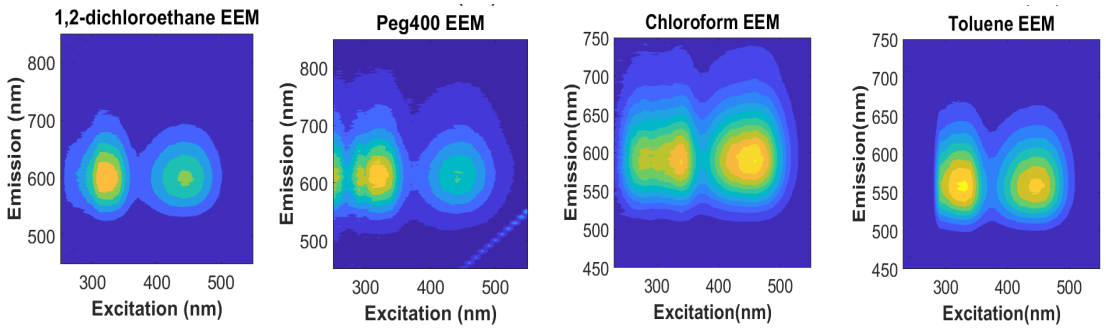

Figure 13 Fluorescence spectra of CBB samples in four solvents: Toluene, Chloroform, PEG 400, and 1,2 Dichloroethane

The data from the EEM spectra are divided into separate plots to simplify analyzing the shifts in the excitation and emission spectra, as shown in Figure 14.

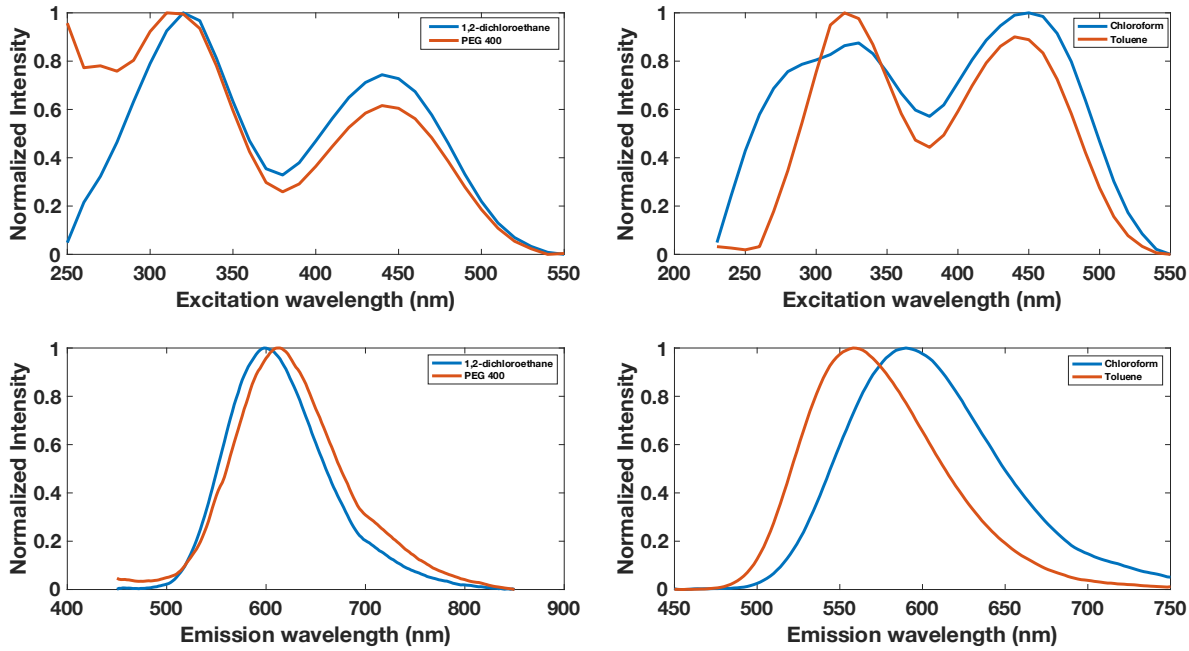

Figure 14 Excitation and emission spectra of CBB dissolved in toluene and chloroform, PEG 400 and 1,2 dichloroethane

Based on research by Seung-Chul Lee et al. (53) , it is evident that changes in fluorescence spectra intensity can be induced by a high-viscosity environment. This shift is a result of the rotation of the dye molecules in a viscous medium, which requires more time compared to in a less viscous environment, resulting in an increased emission lifetime. In other words, the fluorescence lifetimes of TICT fluorophores are directly affected by the viscosity of the medium. In highly viscous solvents, the TICT process slows down, leading to extended fluorescence lifetimes. This phenomenon provides a means of monitoring the viscosity of a medium by observing alterations in fluorescence lifetimes. It is also essential to note that intensity changes are not assessed in this project.

3.1.3 Absorption spectra and oscillator strengths

To determine the absorption behaviour of CBB in solvents with different orientation polarization, CBB is dissolved in acetonitrile and cyclohexane. Absorption spectra are then recorded with a UV-Visible Spectrophotometer (Varian Cary 100 Bio)(see Figure 15). Both solutions with have almost identical absorption spectra in the range of 200 to 600 nm despite having different orientation polarization. The intensity difference is due to different concentrations, 8 ppm and 4 ppm of CBB in cyclohexane and acetonitrile, respectively.

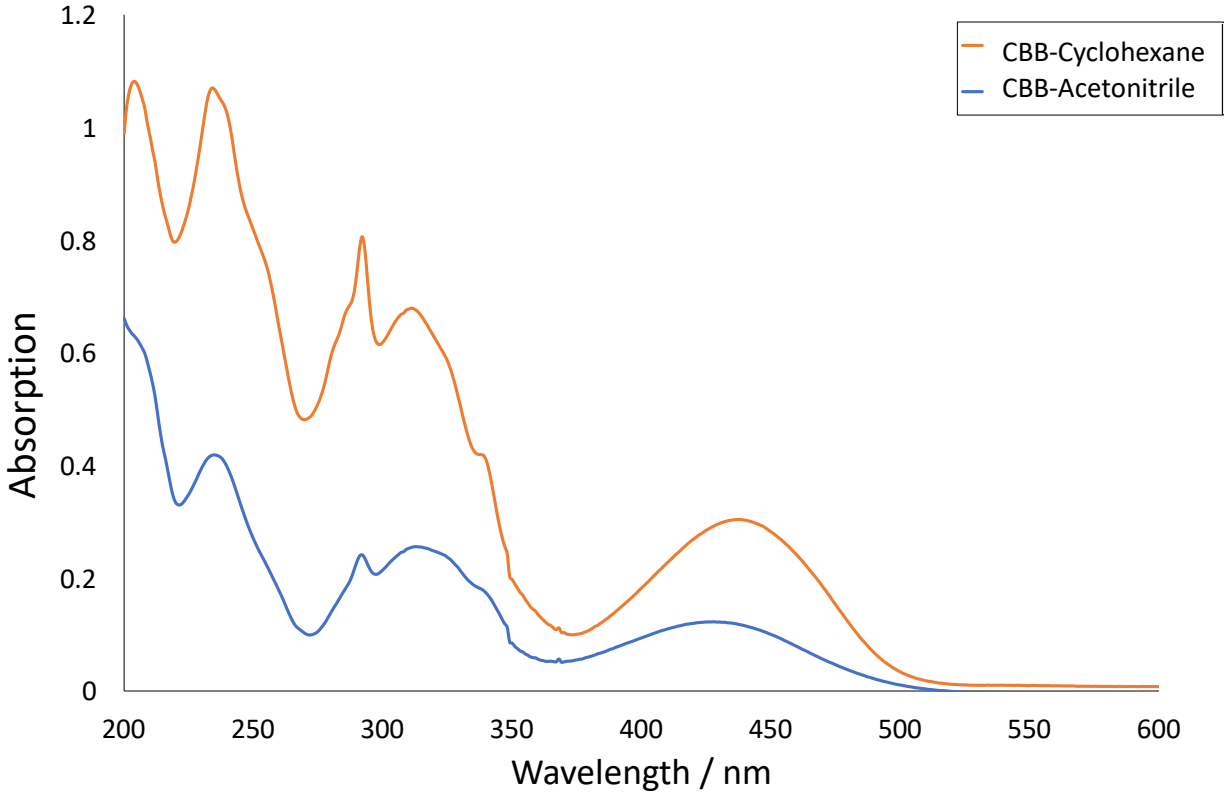

Figure 15 Absorption spectrum of CBB in cyclohexane and acetonitrile

The absorption spectrum of CBB in cyclohexane is fitted to nine Gaussian functions as shown in Figure 21. The estimation of the oscillator strength for the respective transitions is facilitated by integrating the Gaussian fit curves using Eq. 31 (54):

$$f = 4.31\times10^{-9}\frac{cm^2}{L\ mol}\int\varepsilon(\tilde{\upsilon})d\tilde{\upsilon} \qquad 31$$

Results are reported and discussed in section 4.2.

3.1.4 Polarity effect

To show the influence of polarity on the CBB fluorescence emission spectra, the EEM of CBB in acetonitrile and cyclohexane are given in Figure 16.

The fluorescence emission maxima for all absorption processes are centred around 533 nm for cyclohexane and 619 nm for acetonitrile. The EEM maximum at (λ_{Ex} = 341 nm / λ_{Em} = 533 nm) is likely due to the second excited state, S_2, of CBB. According to Kasha's rule, common fluorescence

emission of both S_1- and S_2-states indicates a quick internal conversion process from higher-lying excited states into a common minimum on the S_1 potential energy surface, where fluorescence occurs. This minimum is the focus of this study since its energy above the ground state strongly depends on the solvent polarity. It is anticipated that the molecule in the excited state minimum is strongly dipolar as we observe a strong bathochromic shift in polar solvents (Figure 18 bottom right)

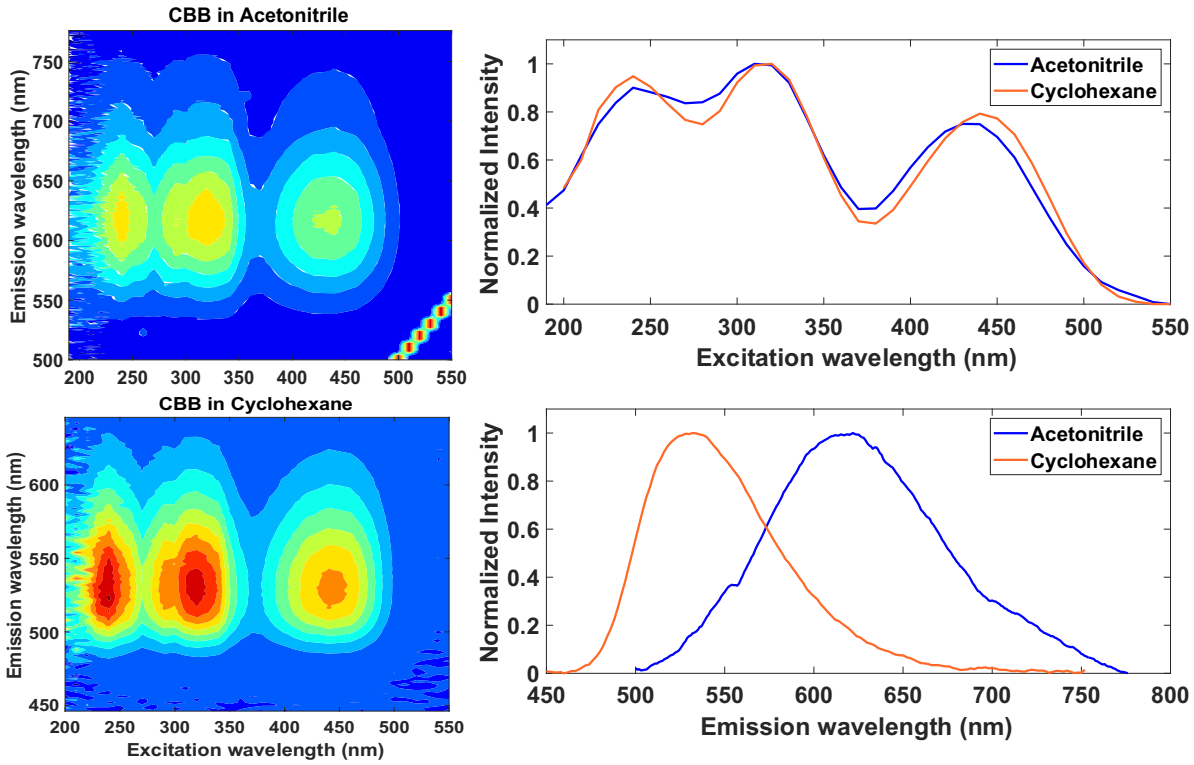

Figure 16 (Left) Excitation-Emission Matrix spectra of CBB in acetonitrile and cyclohexane. The two EEM spectra show three maxima with a common emission spectrum. (Top right) The excitation spectra show three peaks that remain largely unaffected by solvent polarity. (Bottom right) A single peak in the emission spectrum exhibits a strong bathochromic shift as the solvent polarity is increased.

To quantify the solvatochromic effect, a series of samples in which the polarity changes at regular intervals is used. These samples consist of 21 solutions, all with the same concentration of CBB but varying solvent mixtures obtained by mixing a polar and a non-polar solvent. Acetonitrile and cyclohexane would have been preferrable since they are transparent in the UV region of the spectrum, but they are immiscible; instead, acetone and toluene are used. By dissolving CBB in acetone and toluene, two stock solutions in 25.45 ppm by mass concentration are made. Then 21

samples are prepared by mixing the two stock solutions in different proportions. The concentration and polarity of the sample solutions are given in Table 2.

The molar ratio of acetone, MR_{ace}, is determined as follows:

$$\frac{\frac{mR_{ace}}{M_{ace}}}{\frac{mR_{ace}}{Mm_{ace}}+\frac{mR_{tol}}{Mm_{tol}}}=MR_{ace} \qquad 32$$

Where mR: mass ratio and Mm: molar mass

The mass ratio, mR, of Eq.32 is determined as follows:

$$\frac{\left(VR_{ace}\times\rho_{ace}\right)}{VR_{ace}\times\rho_{ace}+VR_{tol}\times\rho_{tol}}=mR_{ace} \qquad 33$$

Where VR: volume ratio and ρ: density.

The molar ratio of CBB, MR_{CBB}, is determined as:

$$\frac{\frac{mR_{CBB}}{Mm_{CBB}}}{\frac{mR_{ace}}{Mm_{ace}}+\frac{mR_{tol}}{Mm_{tol}}}=MR_{CBB} \qquad 34$$

Sample	Volume fraction of Acetone	Molar ratio of Acetone	Molar ratio of CBB (ppm)	Δf
1	0.00	0%	4.24	0.012
2	0.05	7%	4.13	0.031
3	0.10	14%	4.02	0.05
4	0.15	20%	3.92	0.067
5	0.20	26%	3.82	0.084
6	0.25	32%	3.73	0.100
7	0.30	38%	3.64	0.116
8	0.35	44%	3.56	0.131
9	0.40	49%	3.47	0.145
10	0.45	54%	3.39	0.159
11	0.50	59%	3.32	0.172
12	0.55	64%	3.24	0.185
13	0.60	68%	3.17	0.198
14	0.65	73%	3.10	0.210
15	0.70	77%	3.03	0.221
16	0.75	81%	2.97	0.233
17	0.80	85%	2.91	0.243
18	0.85	89%	2.85	0.254
19	0.90	93%	2.79	0.264
20	0.95	96%	2.73	0.274
21	1.00	100%	2.68	0.284

Table 2 *Twenty-one samples of CBB dissolved in a mixture of acetone and toluene*

The orientation polarizations of samples are calculated based on their molar ratio in the sample with Eq.35.

$$\frac{\varepsilon_{r(mix)}-1}{2\varepsilon_{r(mix)}+1}=\left(x_{ace}\times\frac{\varepsilon_{r(ace)}-1}{2\varepsilon_{r(ace)}+1}\right)+\left((1-x_{ace})\times\frac{\varepsilon_{r(tol)}-1}{2\varepsilon_{r(tol)}+1}\right) \quad 35\text{-}1$$

$$\frac{n^2_{mix}-1}{2n^2_{mix}+1}=\left(x_{ace}\times\frac{n^2_{ace}-1}{2n^2_{ace}+1}\right)+\left((1-x_{ace})\times\frac{n^2_{tol}-1}{2n^2_{tol}+1}\right) \quad 35\text{-}2$$

$$\Delta f=\left(\frac{\varepsilon_{r(mix)}-1}{2\varepsilon_{r(mix)}+1}\right)-\left(\frac{n^2_{mix}-1}{2n^2_{mix}+1}\right) \quad 35\text{-}3$$

The calculated orientation polarization, Δf, is given in Table 2.

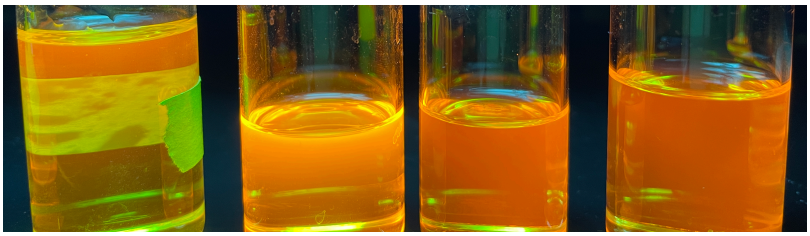

Figure 17 CBB in 100% acetone – 60% acetone - 40% acetone – 100% toluene from left to right

Six representative EEMs out of 21 EEMs of an acetone and toluene mixture are shown in Figure 18.

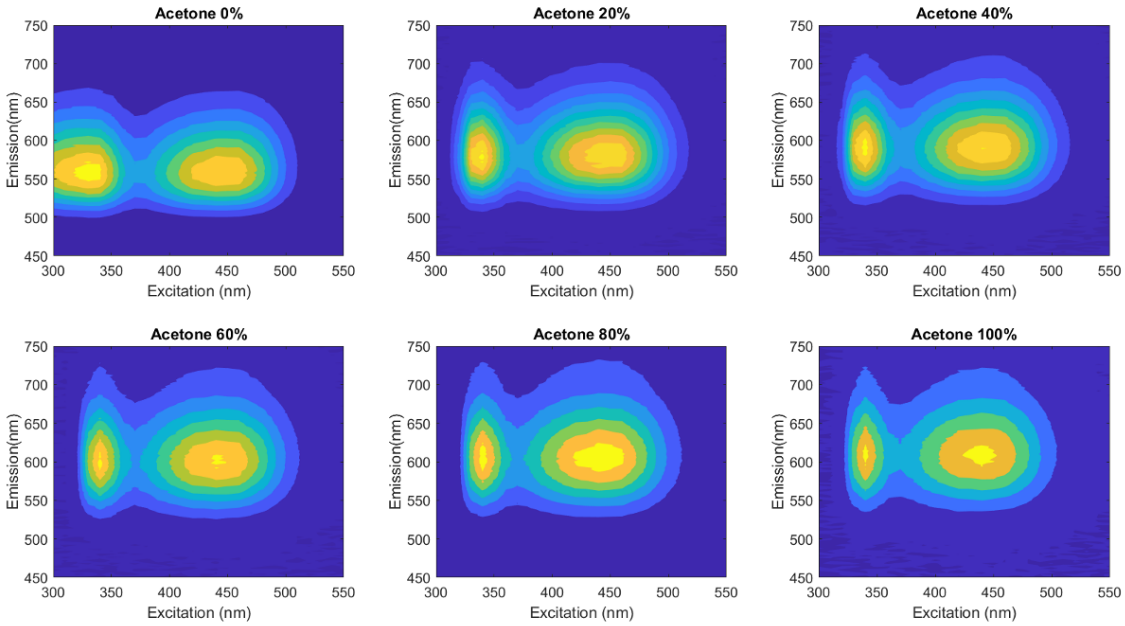

Figure 18 Selected Excitation-Emission Matrix spectra of acetone: toluene mixtures (by volume).

As before in Figure 18 it appears that in all solvent mixtures, the CBB fluorescence at about 600 nm is caused by two excited states, S_2 and S_1, one with an excitation maximum at around λ_{Ex} = 325 nm and the other near 435 nm. Both states exhibit excitation spectra that are remarkably similar (Figure 19), but the centre emission wavelength is 568 nm for toluene and 615 nm for acetone, i.e. we see again a strong bathochromic shift with an increase in solvent polarity.

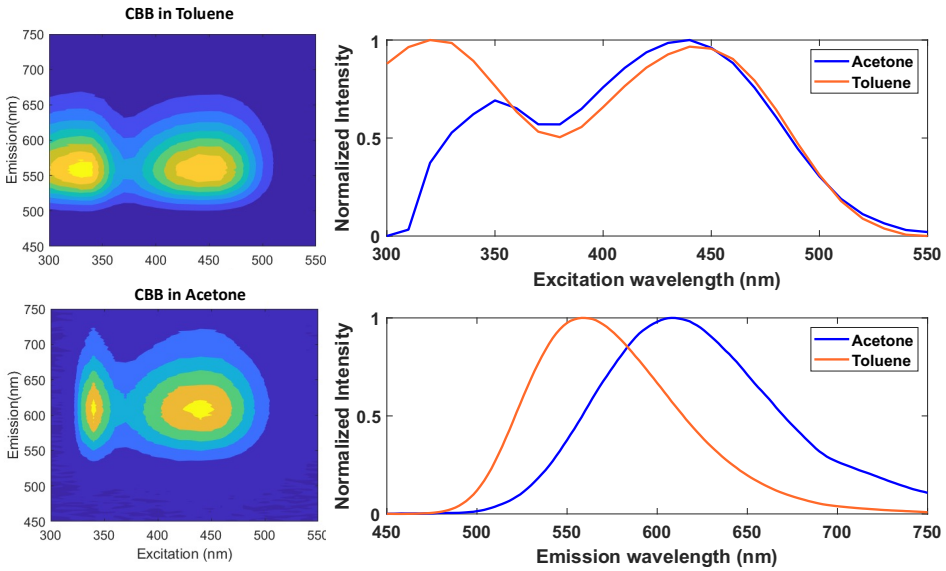

Figure 19 (Left) Excitation-Emission Matrix spectra of CBB in acetone and toluene. The two EEM spectra show two maxima with a common emission spectrum. (Top right) The excitation spectra show two peaks that remain largely unaffected by solvent polarity. (Bottom right) A single peak in the emission spectrum exhibits a strong bathochromic shift as the solvent polarity is increased.

UV light is absorbed by toluene and acetone with cut-off wavelengths of 286 nm and 330 nm, respectively. These cut-offs account for the variations in the CBB excitation spectra in acetone and toluene at $\lambda < 335$ nm as well as for the difference between the EEM spectra in Figure 16 and Figure 18.

Based on these experimental results, the conclusion is drawn that the emission wavelength of this fluorophore shifts due to changes in the polarity of the environment. The reason for this solvatochromic shift is determined next by evaluating the properties of the molecule computationally.

3.2 Computational Method (Corrected Linear Response approach)

To investigate the fluorescence spectrum of CBB and to understand its solvatochromic shift under varying environmental polarities, we develop a method for assessing the molecule's excited energy and dipole moment relative to the ground state within a given solvent. To accomplish this, the computationally corrected linear response approach, cLR, which enables the analysis of the red shift exhibited by CBB in its emission spectrum as a function of solvent polarity, is employed. This method is implemented in the *Gaussian 16* program (55). The cLR approach uses five steps shown schematically in Figure 20:

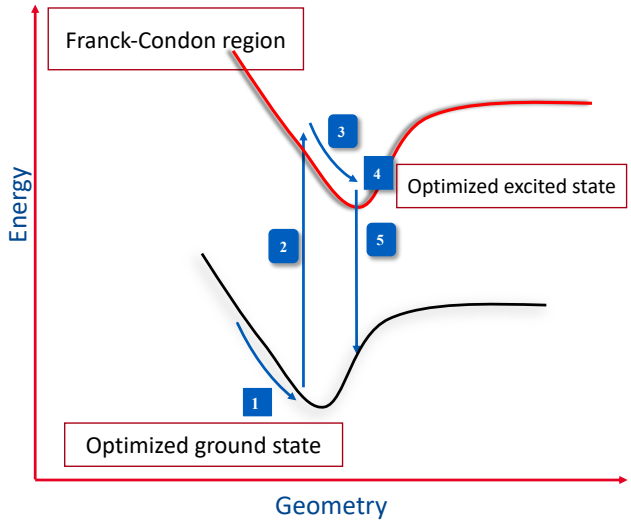

Figure 20 Schematic illustration of the CLR steps

All steps are listed below with a brief description, accompanied by the respective commands given to Gaussian 16 program. The example shown below is for CBB dissolved in acetone. The same process is repeated for toluene.

Step 1: Geometry optimization of the ground state: The ground state structure, S_0, is optimized in this step. To keep the system in its lowest energy state, an attempt is made to optimize the energy gradient for the nuclear positions during the geometry optimization of a molecule's ground state. This is done using density functional theory with the B3LYP/6-31+G (d,p) functional and basis set, along with the integral equation formalism variant of the polarizable continuum model, IEFPCM. As part of this energy calculation, there is an explicit determination of the solvent energy correction due to the local reaction field.

```
#p opt b3lyp/6-31+g(d,p) scrf=(iefpcm,solvent=acetone) polar
```

Step 2: Vertical excitation (absorption): In the initial step, the B3LYP density functional theory (DFT) method is employed to optimize the molecular structure. Subsequently, the optimized configuration is used to evaluate the excited state energy using the CAM-B3LYP functional and Time-Dependent DFT (TD-DFT) calculations. In this step, the optimized structure in the ground state is excited vertically in the solvent model which is generated by the cLR approach in TD-DFT. Here, PisaLR is a synonym for this option. In this example, the calculation is done for four excited states to determine their excitation energy. The state for which the energy and dipole moment between these four excited states are considered is denoted as state 1 (root=1), i.e. the excited state. This step is a vertical excitation, so it is a non-equilibrium calculation in which only the dynamic part of the solvent response partition is equilibrated with the excited state of the solute and the inertial part of the solvent response is still in equilibrium with the ground state energy of solute. The extra input (IOP(10/74=10)) is the necessary for the cLR method to conduct the nonequilibrium calculation. The calculation is performed in a state-specific manner with non-equilibrium solvation.

```
#p td=(singlets,nstates=4,root=1,noneq)
cam-b3lyp/6-31+g(d,p)/def2sv scrf=(solvent=acetone,pisalr)
iop(10/74=10)
```

In the output file, the section "*PCM Corrected Linear-Response - Non-equilibrium solvation*" provides the excitation energy of the molecule with the cLR method.

Step 3: Geometry optimization of the excited state: Before emission, the optimization of its structure in the excited state is performed by using TD-DFT and the CAM-B3LYP/6-31+G(d,p) (IEF-PCM) model. Here, the geometry of the CBB molecule is optimized in the first excited state. In this step, the solvent is equilibrated with solute in the excited state (eqsolv).

```
#p opt td=(singlets,nstates=1,root=1,eqsolv)
cam-b3lyp/6-31+g(d,p)/def2sv scrf=(iefpcm,solvent=acetone)
polar
```

Step 4: Determination of the reaction field of the excited state: Before emission, the reaction field of the solute must converge with the optimized geometry for the solute in the first excited state. For this reason, the state-specific equilibrium solvation of the excited state at its equilibrium

geometry (IOP(10/74=20)) is determined. Solvation information need to be saved for use in the next step (nonequilibrium=save).

```
#p td=(singlets,nstates=4,root=1,eqsolv)
cam-b3lyp/6-31+g(d,p)/def2sv
scrf=(pisalr,solvent=acetone,read,nonequilibrium=save)
IOp(10/74=20)
```

In the output file of this job, the total energy of the molecule which is equilibrated with solvent in the excited state before emission based on the corrected linear response can be found in the section "*PCM State-Specific 1st Order Perturbation Theory - Equilibrium solvation*".

Step 5: Vertical de-excitation (emission): Here, the energy of the ground state is determined using the first excited state optimized geometry (geom=checkpoint) via a non-equilibrium solvation calculation in solution. In addition, the solvent reaction field in equilibrium with the first excited state density (nonequilibrium=read, guess=read) is also calculated. Conformation of the molecule and reaction field of the solvent are determined from the corrected liner-response excited state calculation (oldchk=step4A.chk) in step 4.

```
--link1--
%oldchk=step4A.chk
%chk=step5A.chk

#p cam-b3lyp/6-31+g(d,p)/def2sv
scrf=(solvent=acetone,nonequilibrium=read) guess=read NoSymm
geom=checkpoint polar
```

The ground state energy in the output file is described in the "SCF *Done: E(RCAM-B3LYP)"* section. Finally, the emission energy is obtained by subtracting the energy of step 5 from step 4.

The entire procedure is derived from an article published by Ciro Guido and Stefano Caprasecca, with a few parts modified here due to Gaussian program errors. We believe that the same process can be used to submit new projects for computing the excitation and emission energies of different molecules (2).

It is useful to compare the energies calculated in a solvent environment to those calculated in the gas phase for a non-interacting molecule. The CBB excitation and emission energy in the gas phase is then calculated based on the following job order instruction:

Step 1: Ground state optimization

```
#p opt  b3lyp/6-31+g(d,p)
```

Step 2: Excited state

```
#p td=(singlets,nstates=3,root=1)
cam-b3lyp/6-31+g(d,p)/def2sv density=CI
```

Step 3: Excited state optimization

```
#p opt td=(singlets,nstates=1,root=1)
cam-b3lyp/6-31+g(d,p)/def2sv
```

Step 4: Excited state optimization in the reaction filed

The result is the same as in step 3 because there is no solvent effect to change the energy in step 4.

```
#p td=(singlets,nstates=3,root=1)
cam-b3lyp/6-31+g(d,p)/def2sv Density=CI
```

Step 5: Ground state after emission

```
#p cam-b3lyp/6-31+g(d,p)/def2sv Density=All
```

Chapter 4: Results and discussion

4.1. Validation of the computational method

The cLR computational technique is used to determine the Stokes shift of CBB in different environments and to understand the physical origin of solvatochromic shift of CBB observed in solvent environment with different polarity. Before the results of both computational and experimental data are analyzed, the accuracy of the cLR approach is determined. In **Table 3** the computational and experimental maxima of the fluorescence excitation and emission spectra for CBB dissolved in acetone and toluene are compared.

	Experimental			Computational		
	Toluene	Acetone	Difference	Toluene	Acetone	Difference
$\lambda_{Ex.}$ (nm)	439	433	-6	429	430	1
$\lambda_{Em.}$ (nm)	568	615	47	539	582	43
V_{ss}	5170.3	6828	1658	4757	6074	1317

Table 3 *Experimental and computational excitation and emission energy of CBB in acetone (high polarity) and toluene (low polarity)*

When toluene is replaced with acetone, a near-zero hypsochromic shift of the excitation maximum with increased solvent polarity, i.e., by 1 nm, is calculated. Even though slightly larger, the bathochromic shift of the excitation maxima as experimentally observed (-6 nm) is still within calculation and measurement errors. These results indicate that the excitation (absorption) spectrum does not depend on solvent polarity.

The emission wavelengths are shifted by 47 nm and 43 nm in the experimental and computational results, respectively, as the solvent polarity is increased from toluene to acetone. The same experimental trend is observed when comparing the EEM spectra of CBB in acetonitrile (λ_{em} = 619 nm) and cyclohexane (533 nm). The bathochromic shift of 86 nm is seen in Figure 18 and described in section 3.1.4. Based on this data, the cLR approach is reliable and can be used for these calculations.

4.2. Oscillator strengths based on absorption spectra and calculated data

The estimation of the oscillator strength for the respective transitions is facilitated by integrating the Gaussian fit curves in Table 4 for CBB in cyclohexane using Eq. 31

	Absorption spectrum		**ab initio**	
$S_0 \rightarrow S_n$ (v"→v')	λ_{abs} /nm; E_{abs} /cm^{-1}	f	λ_{abs} /nm; E_{abs} /cm^{-1}	f
$S_0 \rightarrow S_1$	426; 23400	0.02	426; 23400	0.64
$S_0 \rightarrow S_2$ (0→0)	341; 29400	0.001	311; 32100	0.26
$S_0 \rightarrow S_2$ (0→1)	314; 31900	0.064		
$S_0 \rightarrow S_2$ (0→2)	292; 34200	0.002		
$S_0 \rightarrow S_3$ / S_4	284; 35200	0.016	295; 34000 /291; 34300	0.17 / 0.28
$S_0 \rightarrow S_5$	255, 39300	0.049		
$S_0 \rightarrow S_6$	236; 42300	0.029		
$S_0 \rightarrow S_7$	230; 43500	0.060		
$S_0 \rightarrow S_8$	203; 49300	0.204		

Table 4 *Wavelengths, transition energies, and oscillator strengths obtained from Gaussian fits to the absorption spectra of CBB in cyclohexane and acetonitrile, and from ab initio calculations. Values were averaged for the two solvents.*

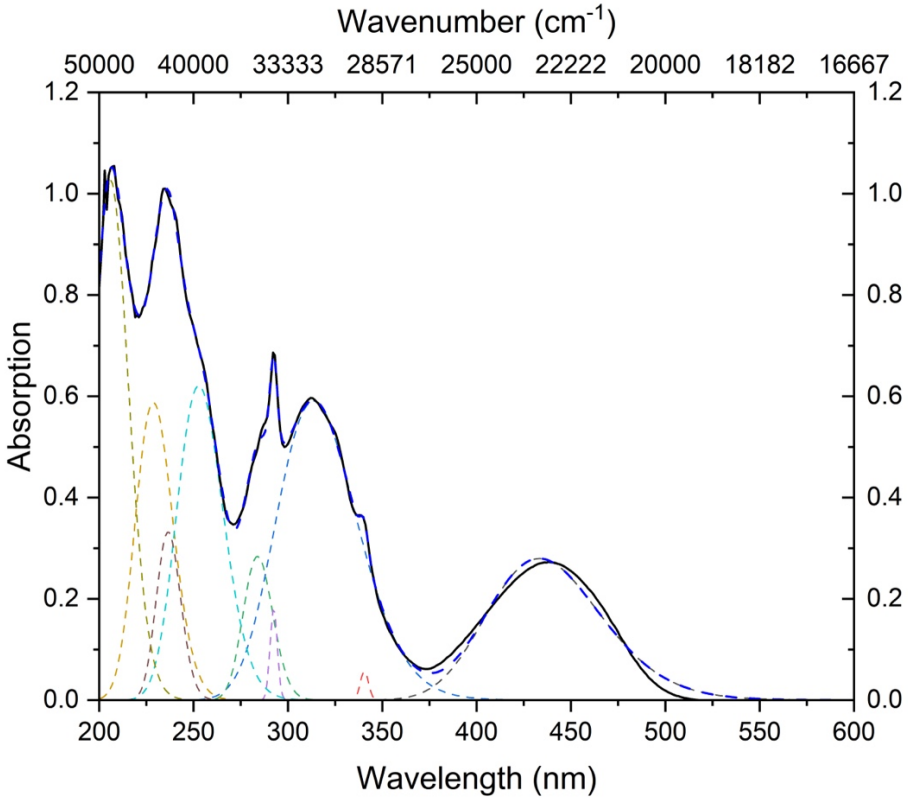

Figure 21 Absorption spectrum of CBB in cyclohexane. The spectrum can be fit using nine Gaussian functions (dashed lines) from which the oscillator strengths in Table 4 were determined.

All transitions in the 200 nm to 500 nm region are due to singlet-singlet transitions. The absorption maximum at 420 nm has been previously attributed to the $S_0 \rightarrow S_1$ transition as described above. The maxima at 341 nm, 314 and 292 nm are likely a vibrational progression ($\tilde{\upsilon}_{0,1} \approx 2500$ cm^{-1}) of the $S_0 \rightarrow S_2$ transition and the maximum at 284 nm could be attributable to either (or both) the $S_0 \rightarrow S_3$ or $S_0 \rightarrow S_4$ transition, which are calculated to be near 295 nm and 291 nm, respectively. Higher-lying transitions could not be reliably assigned. Our TD-DFT calculation found over 30 singlet-singlet transitions below 200 nm, and many were near-degenerate. The absorption maxima in non-polar cyclohexane and the polar acetonitrile are almost identical except for the $S_0 \rightarrow S_1$ transition in which a small difference depending on the solvent $\lambda_{abs(c\text{-}hexane)} = 433$ nm and $\lambda_{abs(MeCN)} = 426$ nm is shown.

4.3. Calculated energy and dipole moments of CBB

In **Table 5**, the CBB energy and dipole moment in toluene, acetone and in gas phase is determined with the cLR approach as described in Chapter 3. Here, $\Delta\mu$ means the difference of the CBB dipole

moment between the excited state just before emission (step 4) and the ground state following emission (step 5) here.

Method	CAM-B3LYP/6-31G+pd							
	μ (D) Step1	μ (D) step2	μ (D) step3	μ (D) step4	μ (D) step5	$\Delta\mu$ (Debye)	Excitation Energy (nm)	Emission Energy (nm)
Gas	2.73	9.34	8.80	8.80	2.83	5.97	418.62	519.65
Toluene	3.28	10.56	10.30	10.30	3.52	6.78	428.50	539.29
Acetone	4.03	12.25	12.05	12.05	5.65	6.40	429.80	582.99

Table 5 *cLR approach result for CBB dissolved in toluene, acetone and in gas phase*

The molecular dipole in the optimized excited state (step 4) is largely unchanged from the dipole in the Franck-Condon region (step 2) in contrast to earlier assumptions that the LE state transforms into a CT state having a much larger charge separation.

In the next section, the computational data from **Table 5** and experimental results from Figure 18 are compared using the Lippert- Mataga equation.

4.4. Lippert-Mataga Equation

To evaluate the solvatochromic effect, 21 samples are prepared by mixing acetone and toluene to dissolve CBB. In the first sample, CBB is dissolved in toluene, which is not very polar. In the last sample, the CBB is in acetone, which is the most polar sample of series. As we go from the first to the last, we increase the amount of acetone and decrease the amount of toluene (**Table 2**).

According to the spectra in Figure 19, the emission wavelength is shifted to the longer wavelengths, as the environment for CBB changes from non-polar (toluene-rich) to high-polar (acetone-rich).

The excitation and emission peaks of EEM spectra for 21 samples are derived from the Gauss2D surface fitting function using the OriginPro application (OriginLab corporation, version 2023b) mentioned in Table 6. The Gauss2D function is as follows:

$$Z = Z_0 + A\exp\left(-\frac{1}{2}\left(\frac{x-x_c}{w_1}\right)^2 - \frac{1}{2}\left(\frac{y-y_c}{w_2}\right)^2\right) \quad 36$$

The function variables are shown schematically in Figure 22 (The figure is extracted from the OriginPro application).

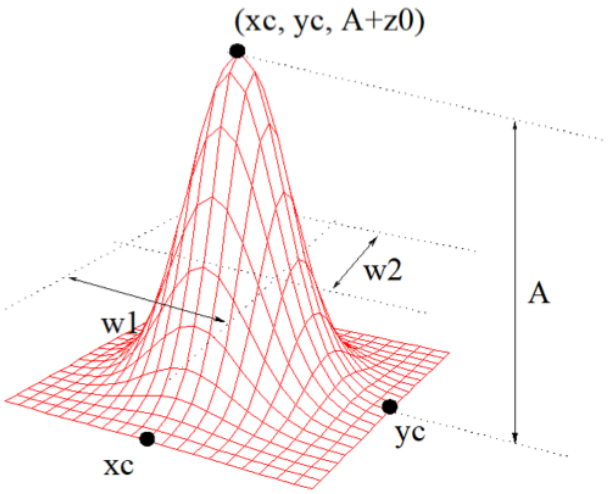

Figure 22 Gauss2D surface function curve

Δf	$\lambda_{Ex.}\ (nm)$	$\lambda_{Em.}\ (nm)$	ν_{ss1}	$\lambda_{Ex.}\ (nm)$	$\lambda_{Em.}\ (nm)$	ν_{ss2}
0.012	323.7	568.0	13290.0	439.0	567.9	5170.3
0.031	336.5	574.8	12319.2	439.1	574.8	5376.0
0.05	337.8	579.1	12331.5	439.2	579.2	5501.2
0.067	338.8	584.3	12404.8	439.2	584.4	5659.1
0.084	339.2	587.5	12457.8	438.8	587.6	5771.0
0.100	339.5	590.0	12501.7	438.8	590.0	5842.1
0.116	339.7	593.2	12576.3	438.6	593.1	5940.8
0.131	340.1	594.8	12592.2	438.5	594.5	5987.5
0.145	340.0	596.5	12648.1	438.2	596.6	6059.1
0.159	341.0	603.6	12758.0	437.4	603.6	6295.7
0.172	340.6	603.1	12778.2	437.2	603.3	6294.8
0.185	340.8	605.5	12831.2	436.3	605.0	6388.8
0.198	340.8	607.9	12891.6	436.2	608.0	6476.8
0.210	340.9	608.1	12894.0	436.3	608.1	6479.0
0.221	341.0	610.5	12950.0	435.4	610.5	6587.6
0.233	340.8	610.5	12966.1	435.3	610.6	6593.3
0.243	340.9	612.1	12998.1	435.1	611.9	6638.8
0.254	340.8	612.6	13022.5	434.5	612.5	6686.8
0.264	340.8	614.1	13053.6	434.3	613.7	6732.1
0.274	340.9	614.6	13068.9	433.6	614.7	6792.9
0.284	340.5	615.2	13115.8	433.2	615.2	6827.9

Table 6 *The excitation and emission peaks of EEM spectra for 21 samples*

This difference in the emission spectra can be explained by considering the dipole moments of CBB and the solvent molecules. The dipole moment of CBB and the dipole moment of the solvent, which is related to its polarity, affect one another. The difference between the dipole moments in the ground and excited states of CBB could be used to examine its sensitivity to polarity. It has been observed that the most sensitive fluorophores are those with the greatest variations in their

dipole moment. This correlation can be estimated from the linearized form of the Lippert-Mataga equation. The Lippert-Mataga equation essentially plots the Stokes shift of the fluorescence emission (in units of energy) against the orientation polarization, i.e. the contribution of the solvent polarization that is not attributable to near-instantaneous electronic polarization.

The Lippert–Mataga equation for evaluating the solvent effect on the Stokes shift (V_{ss} in cm^{-1})(16) is given by:

$$V_{ss} = \frac{2\left(\mu_e - \mu_g\right)^2}{hca^3} \times \sum x_i \left[\left(\frac{\varepsilon_r - 1}{2\varepsilon_r + 1}\right) - \left(\frac{n^2 - 1}{2n^2 + 1}\right)\right] + C \qquad 37$$

where μ_e and μ_g are the CBB dipole moments in the excited and ground states, respectively. The dipole moment unit is Debye (D) which is equal to 1×10^{-18} statcoulomb-centimetres. In this equation, h (= $6.6256 \times 10^{-34}\ kg\ .m^2.s^{-1}$) and c (= $2.9979 \times 10^8\ m.s^{-1}$) are Planck's constant and the speed of light, respectively; a is the Onsager radius of the solvent cavity; ε and n are the relative permittivity and refractive index of the solvent, respectively, and C is the observed Stokes shift of the fluorophore in a non-solvatochromic environment. The term inside the square bracket produces the orientation polarization, Δf. It depends on the relative permittivity and refractive index of the solvent. The Onsager radius, a_0, is the radius of the cavity in which the solute is situated. The units of all the values in the Lippert-Mataga equation are converted to SI units as shown below (orientation polarization is unitless).

$$1\ debye \times \frac{3.3356 \times 10^{-30}\ coulomb\ meter}{1\ debye} = 3.3356 \times 10^{-30}\ C.m$$

$$\frac{\left[3.3356 \times 10^{-30}\right]^2\ c^2 m^2}{1.12\times10^{-10}\ {}^{c^2}/_{Jm}} = 1.0006\times10^{-49}\ \mathrm{Jm}^3 = 1.0006\times10^{-49}\ \ kg.{}^{m^5}/_{s^2}$$

$$4\pi\varepsilon$$

$$\frac{1.0006\times10^{-49}\ \ kg.{}^{m^5}/_{s^2}}{\left(6.6256\times10^{-34}\ \ m^2.Kg.s^{-1}\right)\times\left(2.9979\times10^8\ m/s\right)\times\left(1.5145\times10^{\ -28}\ m^3\right)} = 3326.2039\ m^{-1}$$

h c a^3

Based on the L-M equation, the resultant Stokes wavelength shifts V_{SS2} are graphed against the orientation polarization, Δf in Figure 23

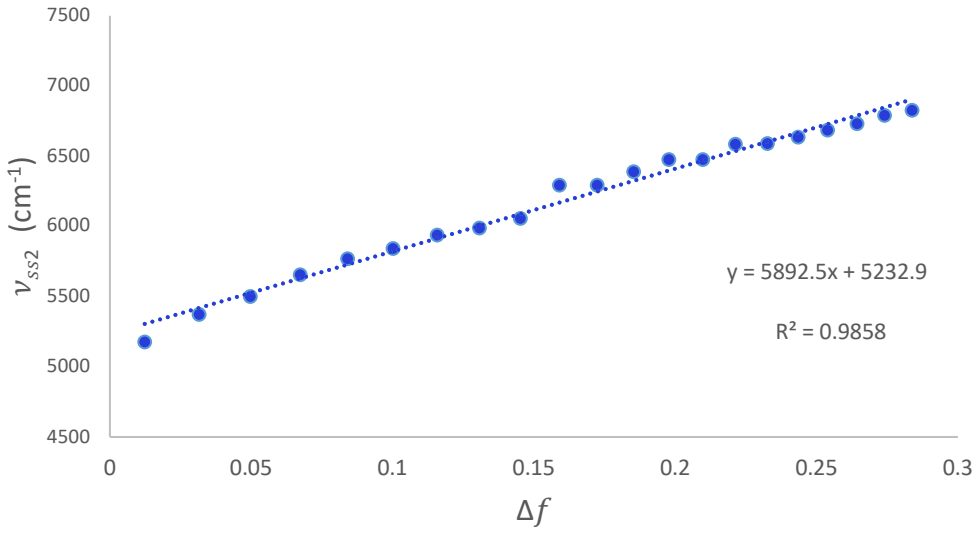

Figure 23 Stokes shift against orientation polarization of twenty-one samples

C is the observed Stokes shift of the fluorophore in a non-solvatochromic environment. The intercept of the linear fitting curve is the experimental C which is equal to 5232.9 cm $^{-1}$, mentioned in **Table 7**. C is also calculated theoretically using the Gaussian program (CAM-B3LYP function using 6-31G+ (p,d) basis set) in the gas phase and is shown in **Table 7**.

CBB in the Gas phase	Excitation (nm)	Emission (nm)	C (cm^{-1})
Theoretical	418.62	519.65	4655.6
L-M fitted curve			5232.9

Table 7 *CBB Excitation, Emission and stokes shift values in the gas phase (non-solvatochromic environment) (The C for L-M fitted curve is extracted from intercept of the linear curve in* **Figure 23***)*

With the L-M Equation, the slope of the curve in Figure 23 should be equal to:

$$slope = \frac{\partial V_{ss}}{\partial \Delta f} = \frac{2\left(\mu_e - \mu_g\right)^2}{hca^3} = 5.89 \times 10^5 m^{-1} \quad (38)$$

To extract dipole moments difference from Eq.38, the constants (h, and c) are applied:

$$\frac{\left(\mu_e - \mu_g\right)^2}{a^3} = 5.85 \times 10^{-20}\, Kg.m^2.s^{-2} \quad (39)$$

The last step to extracting the dipole moment difference is applying the Onsager radius to the equation. This is an ambiguous undertaking and I introduce some models to calculate the radius, as listed below.

First model: Onsager reaction field model

The Onsager reaction field is the simplest theoretical framework used to study the effects of a medium on a solute in chemical reactions. The basic assumption made in this model is that the solute is placed in a spherical cavity inside the solvent. This model is characterized by two parameters: the radius of the cavity and the solvent dielectric constant. The dipole moment of the solute forces the surrounding medium to feel a dipole moment in the opposite direction. The distribution of charges in the solvent is polarised because of the medium becoming polarised. The Onsager reaction field model, as implemented in *Gaussian 16* (SCRF=Dipole), results from treating this mutual polarisation in a self-consistent manner. The produced reaction field in this way is inversely proportional to the third power of the radius of the solute cavity, a_0^3 ,and proportional to the molecular dipole moment (56):

$$\vec{R} = \frac{2(\varepsilon_r - 1)}{2\varepsilon_r + 1} \frac{\vec{\mu}}{a_0^3} \quad (40)$$

R is the reaction field and μ is the molecular dipole moment.

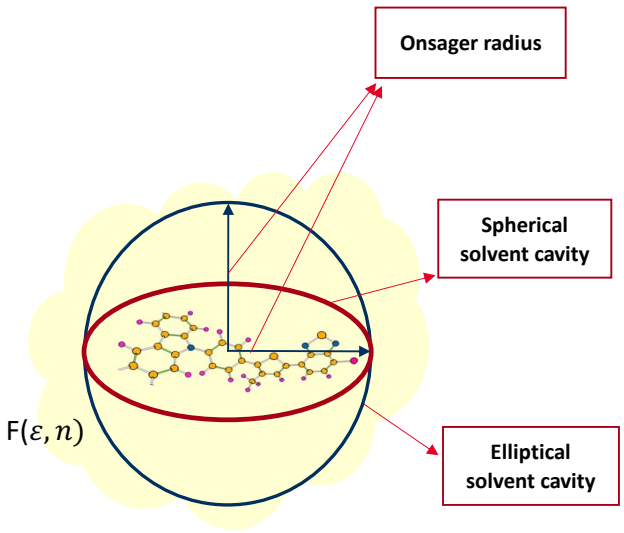

Figure 24 Radius of CBB based on the Onsager model

The CBB molecule under study cannot approximated with a sphere, which seriously calls into question the usefulness of this method as the solvent shell is expected to be elliptical. Using the a spherical domain in this case would cause an overestimation of the dipole moment (57).

Second model: In research by Woyessa et al.(58), the term a_0^3 is replaced with the volume of a solute to adjust for the elliptical shape of the structure and the dependence of the solute cavity on its environmental polarity in the Lippert-Mataga equation. For this reason, the cavity size would be a part of the solvent polarity function:

$$V_{ss} = \frac{2\left(\mu_e - \mu_g\right)^2}{hc} \times \left[\frac{\Delta f}{V}\right] + C \qquad 41$$

Where V is the volume of structure in Eq.41.

Based on this approach, the correct diagram to extract the slope $\frac{2\left(\mu_e - \mu_g\right)^2}{hc}$ is $V_{ss} - C$ versus $\frac{\Delta f}{V}$ instead of the diagram in Figure 23. This diagram needs volume computation for all 21 samples computationally. In this case, it is time consuming to prepare *Gaussian16* input files for many samples with different solvent portions.

Third model: Many papers take the radius as a constant parameter regardless of the solvent polarity effect on the size of the cavity (59) (60) (61) . The radius is computed as follows based on H.Zipse's research:

"….In this way, one much more practical approach consists of calculating the molecular volume as defined through the contour of constant electron density (e.g. at the value of 0.001 electrons/bohr^3), scaling this volume by 1.33 to account for systematic differences between calculated volumes and experimentally measured molar volumes, equating this (non-spherical) molecular volume to the radius of an (ideally spherical) cavity, and adding a constant increment for the closest possible approach of solvent molecules (e. g. 50 pm). This latter approach is used in Gaussian when the "volume" keyword is being used. This indicates that the cavity radius is nothing else but a freely adjustable parameter that defines(62)."

Based on this approach, the radius of CBB is determined using the *Gaussian 16* program (CAM-B3LYP functional using 6-31G+ (p, d)), and equal to 6.12×10^{-10} m. This radius is then used to calculate the dipole moment difference from the L-M equation and compare it with the theoretical dipole moment difference. The results are shown in **Table 8**.

	a_0 (m)	Δμ (Debye) (Restricted model)
Theoretical (Gas phase)		5.97
L-M calculation (For 21 samples)	6.12×10^{-10}	11.58

Table 8 *Dipole moment difference for computational and experimental calculation*

The provided $\Delta\mu$ (the dipole moment difference between excited state and ground state) by this method is twice as large compared to the ab initio calculation because the solvent polarity effect is not considered in calculating the radius.

Fourth model: The PCM model

The PCM (Polarizable Continuum Model) is a computational model used to account for the effect of solvation on the properties of molecules in solution. Therefore, the PCM model is typically applied to molecules in the condensed phase, such as liquids and solids, where the presence of a solvent can significantly affects the behaviour of a solute molecule.

In the gas phase, there is no solvent, and therefore, the PCM model is not applicable. The polarizable continuum model (PCM) using the integral equation formalism variant (IEF- PCM) to determine the cavity volume of CBB in the presence of acetone and toluene for its optimized structure in the ground state with DFT-B3LYP-6-31G+pd and is shown in **Table 9**. The radius of the cavity can be extracted from $V = \frac{4}{3}\pi a_0^3$.

CBB dissolved in	Volume (Å^3)	$a_0^3(m^3)$
Acetone	636.049	1.519×10^{-28}
Toluene	635.803	1.519×10^{-28}

Table 9 *CBB cavity volume in different solvents by PCM model*

The obtained Onsager radius ($a_0 \approx 5.3\ \dot{A}$) can then be used to determine the experimental $\Delta\mu$ (**Table 10**).

$\frac{(\mu_e - \mu_g)^2}{a^3}$ $(Kg.m^2.s^{-2})$	PCM model $a_0^3(m^3)$	$\Delta\mu$ (Debye)
5.85×10^{-20}	1.519×10^{-28}	9.43

Table 10 *CBB dipole moment based on experimental results for twenty-one samples based on the PCM model for radius determination.*

In this section, we have examined the solvent effects on the excitation and emission fluorescence spectra of carbazole–bromobenzothiadiazole. The dipole moment difference between the ground and excited state of fluorophore is determined using the Lippert–Mataga equation and the $\Delta\mu$ is 9.43 Debye. The obtained diagram of the Stokes shift versus orientation polarization for the experimental data based on Table 1 and Table 6 is compared with the equivalent diagram from

Chernick's published paper about CBB dissolved in different solvents in Figure 25. The experimentally obtained slope by Chernick et al. $\frac{dv_{ss}}{d\Delta f} = 4.840 \times 10^5$ m^{-1} yields $\Delta\mu \approx 8.5$ D (1).

Theoretical μ_g and μ_e have been determined by quantum chemical calculations using DFT-CAM-B3LYP/6-31G+(p, d) and TD-DFT- CAM-B3LYP/6-31G+ (p, d) level of theory and $\Delta\mu$ is almost 5.97-6.78 Debye according to **Table 5**. The dipole moment for the CBB in the excited state is higher than that of the ground state in the calculations, revealing that the molecule is polarized in the excited state in comparison with the ground state.

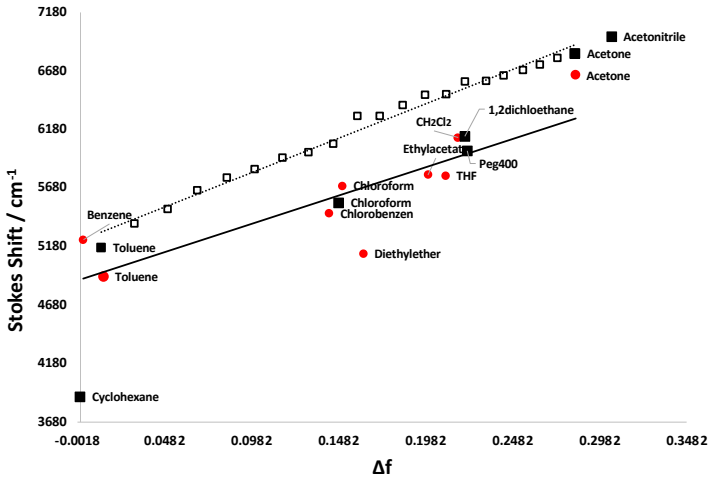

Figure 25 Lippert-Mataga plot showing the solvatochromic Stokes shift, V_{SS}, as a function of the solvents' orientation polarization. CBB was dissolved in 19 toluene-acetone mixtures (open squares) and 7 neat solvents (solid black squares). Previously recorded V_{SS} are included (red circles). Linear fit curves to the neat solvents are shown as a solid lines and to the mixtures with dashed line (1)

These dipole moment values are somewhat consistent with each other, but they are notably lower than what one might anticipate for an excited state with complete charge separation. To put it into perspective, a fully charge-separated excited state, with a separation of, for instance, 9 Å (equivalent to the distance between 6 carbon-carbon bonds), would yield a dipole moment of approximately 45 Debye (D). Even if a partial charge separation between the donor and acceptor components in CBB is considered over a relatively long distance, dipole moments larger than 20 D are still anticipated. However, significantly smaller charge separation within the acceptor moiety alone is suggested by our ab initio calculations as will be shown below.

It is crucial to keep in mind that the Lippert-Mataga model has known drawbacks (24). The calculated dipole moment is significantly influenced by the value of the Onsager radius. Based on

ab initio calculations, our estimate of a_0 = 5.3 may have several percents of margin of error. Additionally, the orientation polarization term, Δf, has been studied extensively, resulting in several variations of the equation for evaluation (58, 63). Furthermore, literature evidence indicates that the local solvent environment differs from what one might expect from a statistical distribution of solvent molecules around the solute (64). In this case, the more polar acetone likely forms a solvent cage around the solute which is not easily displaced by toluene. Due to this effect, acetone may contribute more to the solvent cage even at low acetone concentrations, changing the polarization term to one that is more "acetone-like." The data in Figure 23 align along a slightly curved line to support this theory. It is also important to note that commonly used equations derived from the Lippert-Mataga model ignore the impact of a solvent-induced dipole. As a result, the solvent polarity affects the solute dipoles in both the excited and ground states, and an additional term is needed to account for the strength of short-range dispersion interactions. Highly conjugated linear molecules, such as those made for TICT states, are likely to exhibit a more pronounced effect in this regard. This effect is influenced by the polarizability of the solute.

4.5. Computational method

The energy of CBB through the excitation and emission processes is calculated in the gas phase and in acetone and toluene solvent environments using TD-DFT calculation via the cLR approach as mentioned in Table 11. Calculation of total CBB energy for both spin-restricted and unrestricted electron configurations are performed. The calculated energy differences between restricted and unrestricted calculations are negligible, and all results reported here are therefore obtained using the faster spin-restricted calculations.

The emission wavelengths of CBB in the two solvents are determined and compared to experimental values. The calculated emission wavelengths of 540 nm (18500 cm^{-1}) in toluene and 582 nm (17200 cm^{-1}) in acetone are consistent with the experimental values of 568 nm (17,600 cm^{-1}) in toluene and 615 nm (16,300 cm^{-1}) in acetone. We note that the calculated value for the bathochromic shift of 1360 cm^{-1} agrees nearly perfectly with the experimental value of 1350 cm^{-1}, thus indicating that the cLR model provides an accurate representation of the solvent effects.

		(1)	(2)	(4)	(5)	(2)-(1)	(4)-(5)
Theory E (cm^{-1})	Gas	0	23888	21372	2129	23888	19244
	Toluene	-1272	22064	19625	1110	23337	18515
	Acetone	-2758	20508	17532	379	23266	17153
Expt. E (cm^{-1})	Gas						
	Toluene					22779	17609
	Acetone					23084	16255

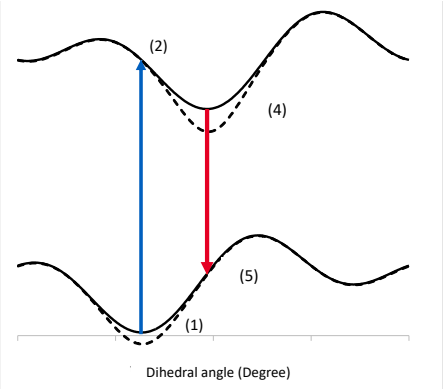

Table 11 *Calculated energies of CBB in the gas phase and two different solvent environments acetone, and toluene to compare with experimental results. Values were determined for the ground state, (1), and the excited state, (2), through the excitation and for the ground state, (5), and the minimum excited state, and (4), through the emission.*

The ground state equilibrium configuration of CBB and respective dihedral angles are illustrated in Figure 26. Three dihedral angles, θ_1, θ_2, and θ_3, are responsible for most of the geometry changes between the minima of the ground state and excited state potential energy surface and their values are reported in Table 12.

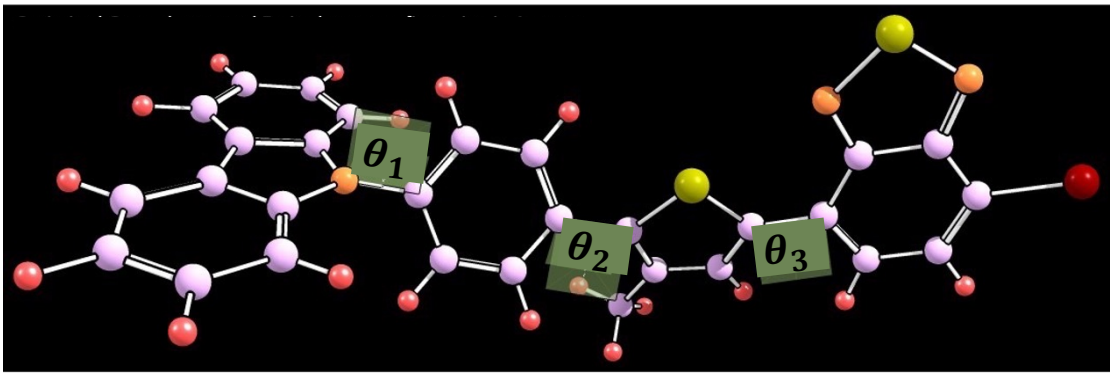

.

Figure 26 Dihedral angles of CBB

		Franck-Condon Region	Fluorescence Region
θ_1	Gas	58.83	51.77
	Toluene	60.62	51.82
	Acetone	60.95	51.93
θ_2	Gas	42.63	30.32
	Toluene	42.35	28.48
	Acetone	41.45	27.81
θ_3	Gas	-16.43	-0.76
	Toluene	-16.53	-0.63
	Acetone	-15.82	-0.42

Table 12 *Calculated dihedral angles of CBB in the gas phase and two different solvent environments. Values were determined in the Franck-Condon Region and the emission region*

It is crucial to highlight that the configuration at the excited state minimum does not show a significant twist in comparison to the lowest energy point of the molecule in its ground state. This is different from our original anticipation for the formation of a TICT state. Instead, it appears that the molecule in the excited state is just a bit closer to being planar. The reason for the solvatochromic shift is discussed in further detail in the following section, by evaluating the potential energy surface, dipole moment, and occupancy of electrons in molecular orbitals of CBB based on the changes in the dihedral angles.

4.6. The solvatochromic shift

Potential energy surface: Representative 2D S_1-excited state potential energy surfaces (PES) of CBB in acetone are plotted as a function of its dihedral angles to survey the potential energy surface around the S_1 minimum by twisting the molecule around two dihedral angles while the third dihedral angle is frozen (Figure 27). The red points indicate the energy of the molecule in the Franck - Condon region, i.e. the ground state minimum configuration, and the white points indicate the energy of the molecule in the optimized excited state. In these surfaces, there is no barrier or a TICT minimum near the S_1 minimum in the excited state and the energy level of the molecule is decreased from the Franck-Condon region to the optimized excited state slightly without moving another local minimum energy barrier on the surface. The calculations for CBB in acetone are presented as the chosen solvent for stabilizing the TICT state. Interestingly, remarkably similar results are produced by S_1 potential energy scans in alternative solvents.

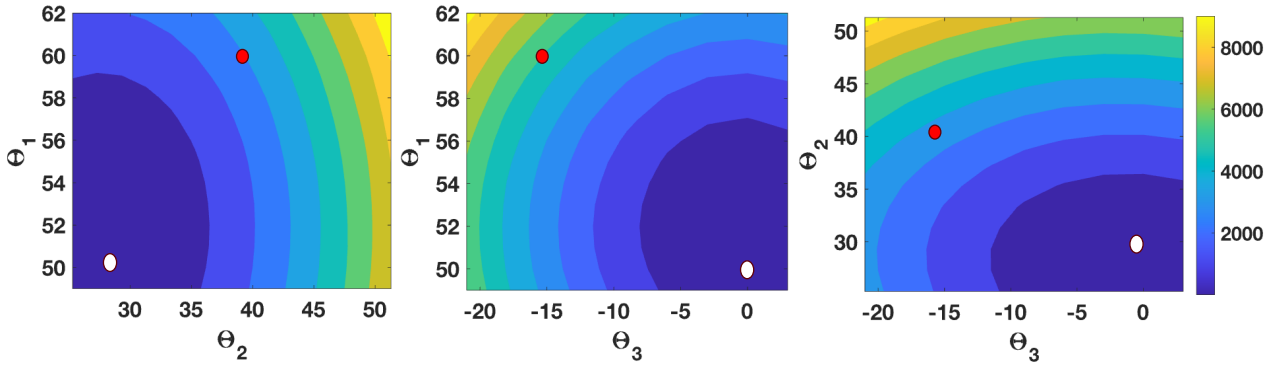

Figure 27 Two-dimensional PES of CBB in acetone. The red dot at θ_1 = 61.00, θ_2 = 41.40 and θ_3 = -15.80 signifies the Franck-Condon region and the white dot at θ_1 = 51.90, θ_2 = 27.80 and θ_3 = -15.40 signifies the minimum of S_1 from where emission occurs. The colour bar indicates the energy above the minimum in units of cm^{-1}.

The energy of CBB in acetone around the optimized excited state by a wide scan of all dihedral angles is determined and is plotted in Figure 28 to assess the presence of a TICT state at 90°. Each

angle is scanned while the other two dihedral angles are in their excited state minimum configuration. Changing the dihedral angle,θ_3, resulted in a large increase in dipole moment and, in both solvents, in a second narrow energy minimum at θ_3=90^0. In addition, due to the third dihedral's proximity to the acceptor part, where the main charge transfer occurs along the fluorescence process, the third dihedral angle dominates the reaction coordinate.

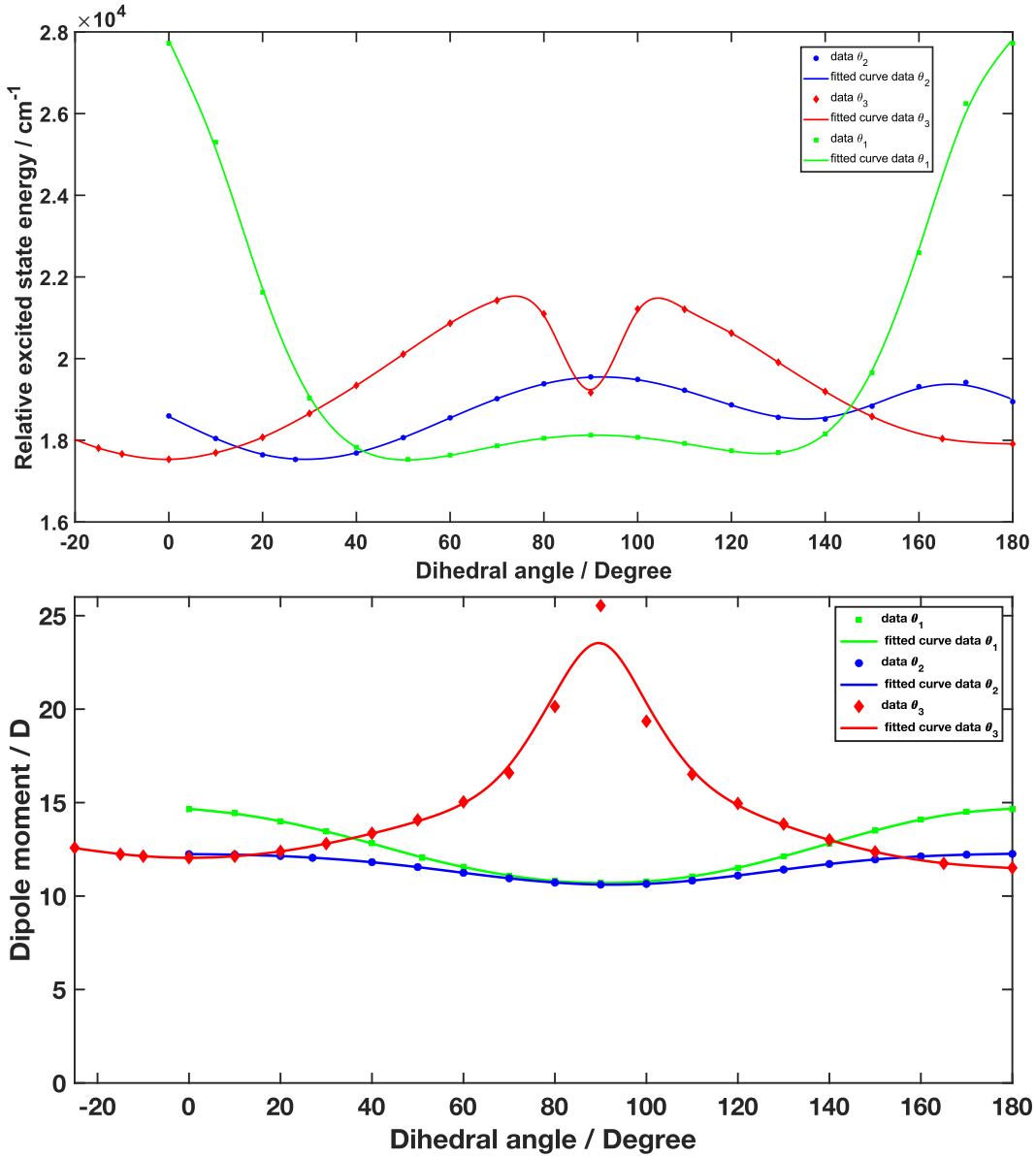

Figure 28 S_1-state energy (top) and dipole moment (below) of CBB in acetone calculated as functions of dihedral angles θ_1, θ_2, and θ_3. The respective other coordinates were held at their S_1 state minimum values, i.e. θ_1 = 52^0, θ_2 =28^0, and θ_3 = 0 ^{0}.

The θ_3 angle is then scanned in both acetone and toluene and the gas phase. The PES of CBB in acetone (polar environment), toluene (non-polar environment) and gas phase (non-

solvatochromic environment) are plotted in the excited state (before emission) and ground state (after emission) in Figure 29.

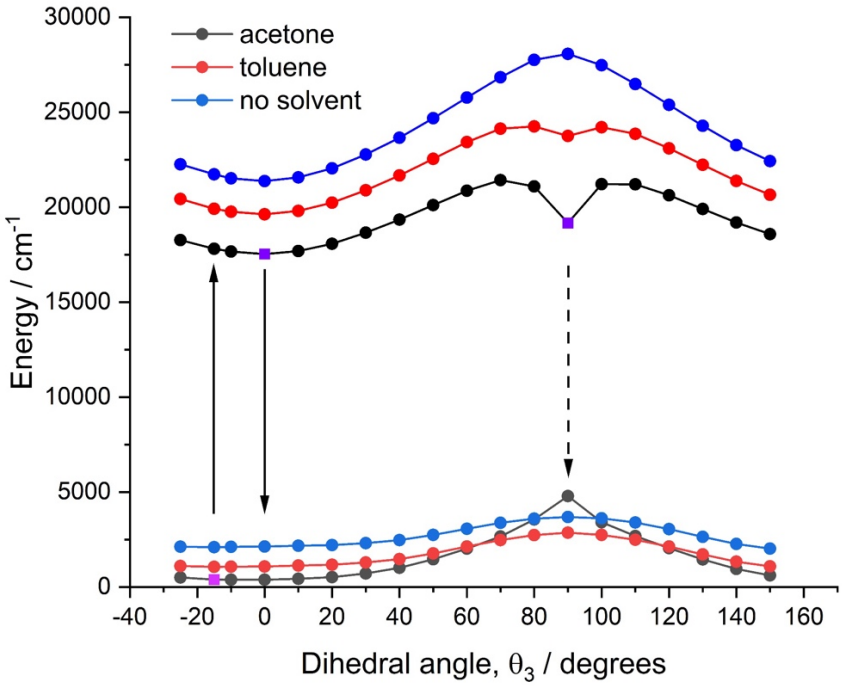

Figure 29 Energy of CBB in acetone in excited state and ground state in the emission region. Energies are given for the ground state minimum of an isolated CBB molecule.

The energy of the molecule in the gas phase is increased in the excited state when the third angle is at 90°, but the energy decreases in the presence of a solvent (either acetone or toluene) in the system. Based on these results, the S_1 potential of CBB in acetone and toluene shows a second minimum at a higher energy corresponding to a θ_3= 90° far away from the global minimum of the S_1 state. Interestingly, the depth of the minimum depends on the solvent's polarity. This second minimum at θ_3= 90^0, corresponds to the TICT conformation.

We then optimized the conformation of the CBB by keeping θ_3 fixed at 90^0 , i.e. we allowed the molecule to relax when placed in the TICT state (Table 13). During this process, it is observed that θ_1 and θ_2 convert to around 45^0 and 21 - 25^0, respectively, while θ_3 is locked at 90^0 when CBB is in the TICT state. θ_1 and θ_2 are therefore close to their values at the global minimum of the excited state (as seen in Table 12), confirming that θ_3 is indeed the most meaningful reaction coordinate.

The second, local energy minimum at $\theta_3 = 90^0$ is believed to correspond to the TICT state because the CBB dipole moment is over 25 Debye based on computational method, as would be the case if more than half a unit charge are to separate by over 9 Å.

		TICT $\boldsymbol{\theta_3 = 90°}$	Planer $\boldsymbol{\theta_3 = 0°}$
$\boldsymbol{\mu/D}$	Gas	23.7	8.8
	Toluene	25.6	10.3
	Acetone	27.2	12.0
Theory E /cm^{-1}	Gas	27779	21400
	Toluene	23238	19600
	Acetone	18361	17500

Table 13 Calculated dipole moments and S_1-state energies of CBB in the gas phase and in two different solvent environments. Values were obtained by using TD-DFT with CAM-B3LYP/6-31G+pd to optimize the rest of the confirmation while freezing the $\boldsymbol{\theta_3}$ at the TICT conformation ($\boldsymbol{\theta_3}$ = 90^0) and at the $\boldsymbol{\theta_3}$ = 0^0 of the S_1 state.

Dipole moment: By altering the third dihedral angle, the dipole moment of CBB is calculated in the acetone, toluene, and gas phases while dihedral angles θ_1 and θ_2 are fixed at the S_1-minimum conformation. The molecule's dipole moment increases by increasing the polarity of the environment based on Figure 30 in both ground and excited states. The increase in the dipole moment value in polar solvents can be attributed to the induced dipole contributions. This is a result of the high polarizability of the CBB molecules, especially along their primary axis (65).

In addition, the dipole moment is increased dramatically when θ_3 is varied from 0° to 90°.

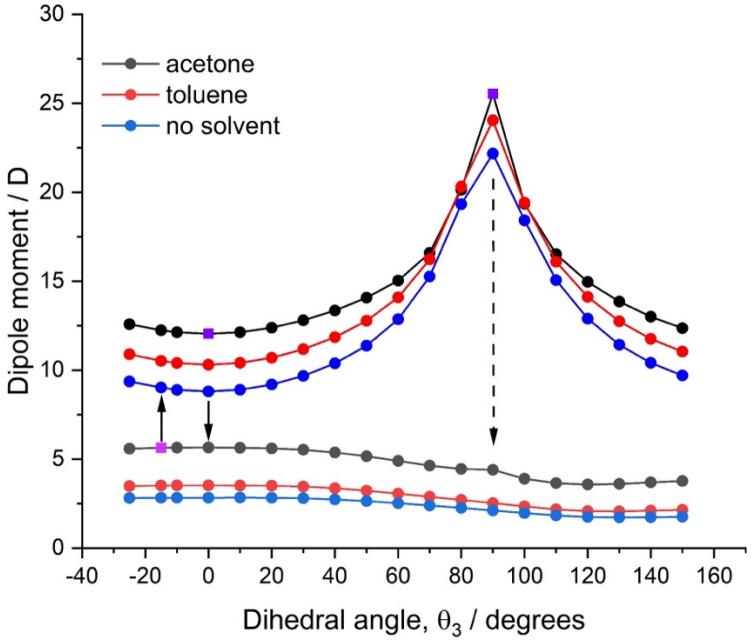

Figure 30 Dipole moment of CBB in different environments in the excited state and the ground state after emission by changing the third dihedral angle

Figure 31 shows the dipole moment vectors of CBB in acetone in the excited state when θ_3 is 0° and 90° and the other angles correspond to the excited state minimum conformation. The dipole moment points along the molecular long axis and toward the acceptor section in the TICT state ($\theta_3 = 90^0$) in contrast to the minimum excited state ($\theta_3 = 0^0$) when the dipole moment is nearly orthogonal to the molecular axis.

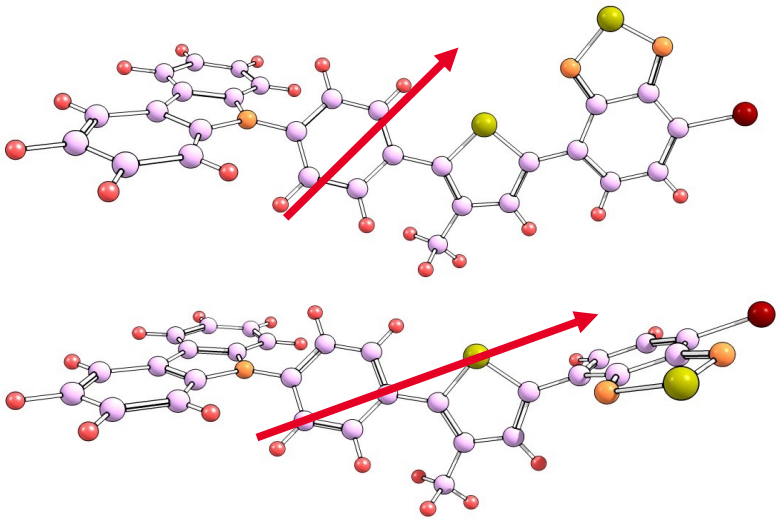

Figure 31 Conformations and dipole moment vectors of CBB in acetone calculated at the S_1 minimum, θ_3 = 0 °, and in the TICT conformation at θ_3 = 90 ° before emission (from top).

According to the results in Figure 29, while varying the θ_3 from 0° to 90°, the excited state energy (in the presence of a solvent) initially increases and then decreases , i.e. there is a solvent-dependent barrier to rotation around θ_3, which is found near the twisted confirmation. The molecular dipole moment at 90° is also greater than 0° in the excited state based on Figure 30. The combination of these two results provides reasonable evidence that a TICT state exists in the presence of a polar solvent. On the other hand, the energy at 90^0 is greater than the 0^0 in the excited state in Figure 29 (**Table *13***) and the Franck-Condon region is close to the global excited state minimum near the planar conformation. Together these factors suggest that even though there is a TICT state, the fluorescence emission does not originate from the TICT state. This is accordance with Kasha's rule, starting that fluorescence emission usually comes from the lowest excited state.

In the above calculation all PES are calculated using the "rigid scan" option in the Gaussian program. In the rigid scan, all atoms and bonds are fixed in the optimized excited state configuration and only the chosen dihedral angles are rotated. The molecular geometry must be defined in Z-matrix in the rigid scan. The Z-matrix defines the position of atoms relative to previously defined atoms using a length, an angle, and a dihedral angle.

```
#p scan td=(singlets,nstates=1,root=1,eqsolv)
cam-b3lyp/6-31+g(d,p)/def2sv
scrf=(pisalr,solvent=acetone,read,nonequilibrium=save)
IOp(10/74=20)
```

Molecular orbitals: Dipole moment changes occur when a molecule is excited because of a rearrangement of charges within its structure. This means that electrons move from one part of the molecule (the donor) to another part (the acceptor). When the molecule is excited, electrons transfer from occupied orbitals to the unoccupied ones. The electron transfer during excitation enables the analysis and interpretation of changes in the molecular charge distribution. Previous observations have been confirmed by our *ab initio* calculations that the transition from the ground state (S_0) to the first excited state (S_1) is primarily driven by two key transitions: HOMO to LUMO, and the HOMO-1 to LUMO transitions, with each contributing roughly 50% to the overall electronic transition. The output file for the excited state CBB is shown below:

```
 Excitation energies and oscillator strengths:

 Excited State   1:      Singlet-A      2.9122 eV  425.74 nm  f=0.6207
<S**2>=0.000
     139 ->141        -0.41951
     140 ->141         0.54620
```

The primary transition leading to the first excited state involves orbitals 139 (HOMO-1), 140 (HOMO), and 141 (LUMO). Using ChemCraft, canonical orbitals for the first excited state of CBB are poltted, as depicted in Figure 32. The canonical frontier orbitals indicate that the wavefunction is localized near the donor group in the two occupied MOs and shifts to the acceptor group in the LUMO. It is also shown by diagrams that the HOMO wavefunctions on the carbazole (donor group) are nearly identical. However, more noticeable differences in the HOMO wavefunctions can be observed in the linker groups and the bromobenzothiadiazole (acceptor).

For CBB in acetone, the $S_0 \rightarrow S_1$ transition can be described as -0.42× (HOMO-1) + 0.55× (HOMO) → LUMO. Since both HOMO orbitals contribute roughly equally but with opposite signs, the portion of the HOMO wavefunctions located at the donor group largely cancels out.

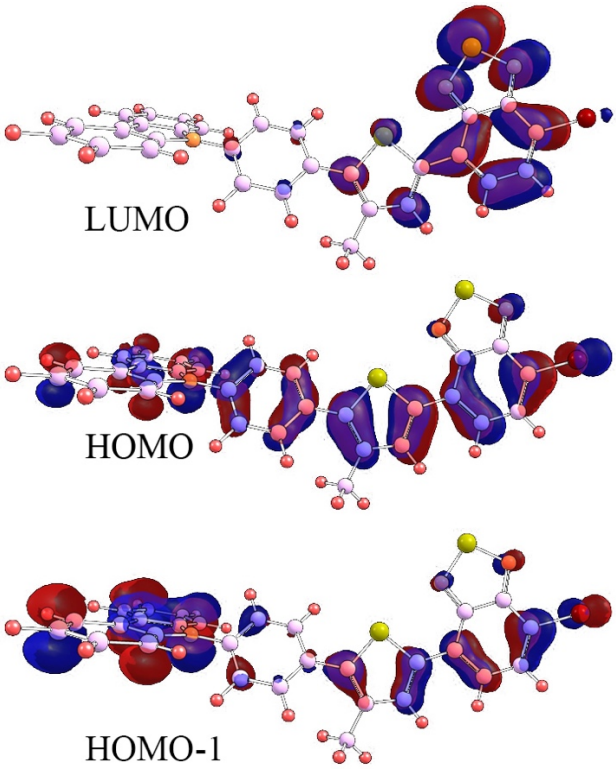

Figure 32 The canonical frontier orbitals of CBB in the gas phase are determined at the minimum of the S_1 state. The $S_0 \rightarrow S_1$ transition involves electronic transitions from the difference between the two HOMOs into the LUMO

Computing Natural Transition Orbitals (NTOs) is a more valuable tool for gaining a deeper understanding of electron transitions. These NTOs, as shown in Figure 33 and calculated using *Gaussian 16* program, provide a way to transform the occupied and virtual molecular orbitals (MOs) into two sets of occupied and virtual MOs that enable the description of the transition as a "particle-hole excitation."(66). Each hole, characterized by an occupied NTO, is paired with a corresponding particle NTO in the virtual space. The approach using NTOs offers a more intuitive representation of the excitation process.

In our case, the transition from the ground state (S_0) to the first excited state (S_1) involves only a single NTO-HOMO/LUMO pair. Interestingly, neither of these NTOs is predominantly located at the designated donor group of the molecule. The dipole moment in both the ground and excited states does not show a significant charge separation between the donor and acceptor, which is consistent with our observation of a small dipole change upon excitation and is a unique benefit of using the NTO approach. The two sulphur atoms in the benzothiadiazole acceptor and the

phenylthiophene bridge, instead, appear to receive some of the electron density that was previously occupied by the bromine substituents.

The NTO for the first transition state is generated with below job order using the data from checkpoint file of the first excited state calculation.

```
#p td=(singlets,nstates=3,root=1) cam-b3lyp/6-31+g(d,p)/def2sv Geom=All Check
Guess=(Read,Only) Density=(Check,Transition=1) Pop=(Minimal,NTO ,SaveNTO)
```

In the NTO checkpoint file, it can be observed that the numbers next to the orbitals are their occupation numbers associated with the first state, not their energy, so only those need to be plotted for a more comprehensive description. Compared to all the different combinations given in the canonical basis from the direct TD-DFT calculation, the NTO transition 140->141 is much simpler to understand.

```
Excited State   1:      Singlet-A      0.0000 eV    0.00 nm  f=0.0000  <S**2>=0.000
    140 ->141         0.35355
    140 <-141         0.35355
This state for optimization and/or second-order correction.
Total Energy, E(TD-HF/TD-DFT) =   0.00000000000
Copying the excited state density for this state as the 1-particle RhoCI density.
```

The natural transition orbitals for the first excited state are plotted in Figure 33 for CBB. The carbazole donor group is not involved in the electron transition during excitation and all charge transfer is from the bridge to the benzothiadiazole acceptor group at coplanar configuration, $\theta_3 = 0^0$, when θ_3 is fixed to 90^0 the charge transfer is from the carbazole (CBz) donor (with contributions of both linker groups) to the benzothiadiazole acceptor group. This is consistent with the large dipole moment along the long axis of the molecule at $\theta_3 = 90^0$.

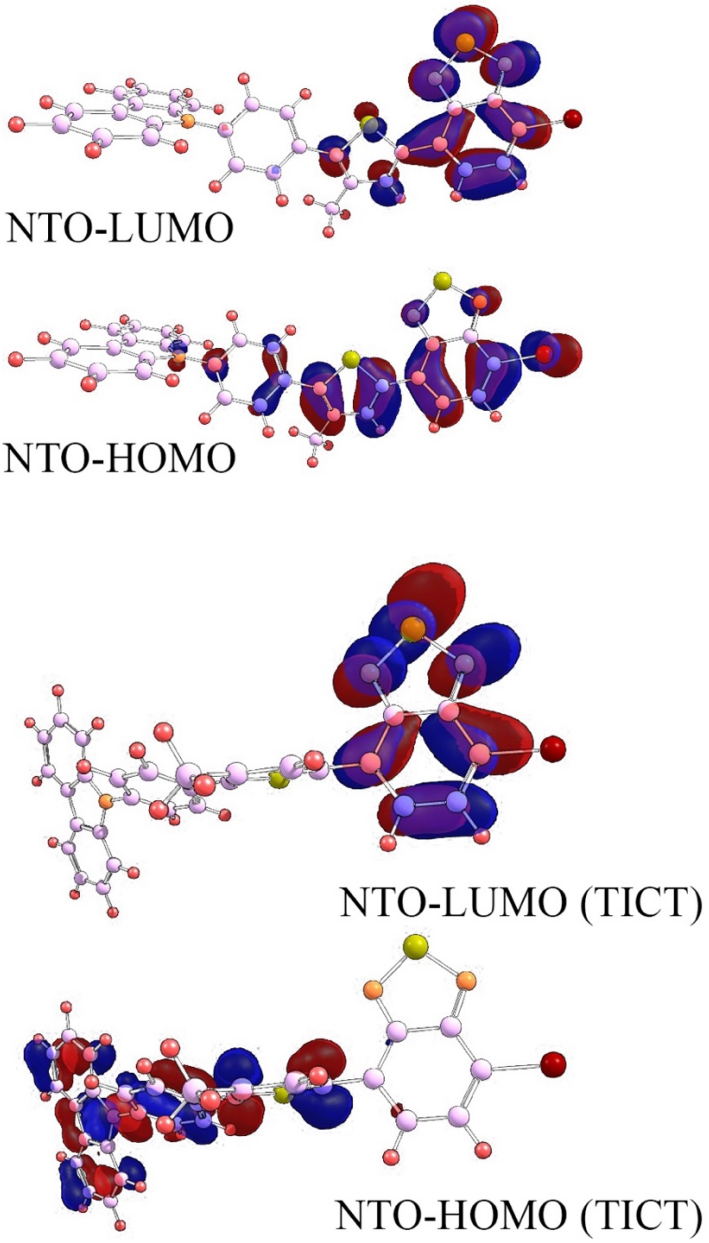

Figure 33 Natural Transition Orbitals for CBB. Orbital 140 (Homo) and Orbital 141 (Lumo) exhibit the largest occupations for the first excited state

Based on this finding, it is simple to conclude that when CBB in acetone is excited from its ground state, electrons from the phenylthiophene (PT) bridge and from the bromine atom are transferred to the benzothiadiazole (acceptor group) when θ_3 is close to 0^0, whereas when a molecule is twisted, $\theta_3 = 90^0$, the donor group is included for charge distribution as well. This statement is visualized as an electron density distribution map in Figure 34. Within the cLR approach, the

emission occurs from the coplanar form of CBB to reach the ground state and it does not have donor to acceptor charge transfer during emission. To show this electron distribution, the excited state electron density cube is generated (CI) and the electron density difference between the excited state and ground is calculated. The electron density difference cube is mapped onto the SCF electron density surface. The blue region is the positive value of the density difference where the excited state density is larger than the ground state and the red region indicates the reverse.

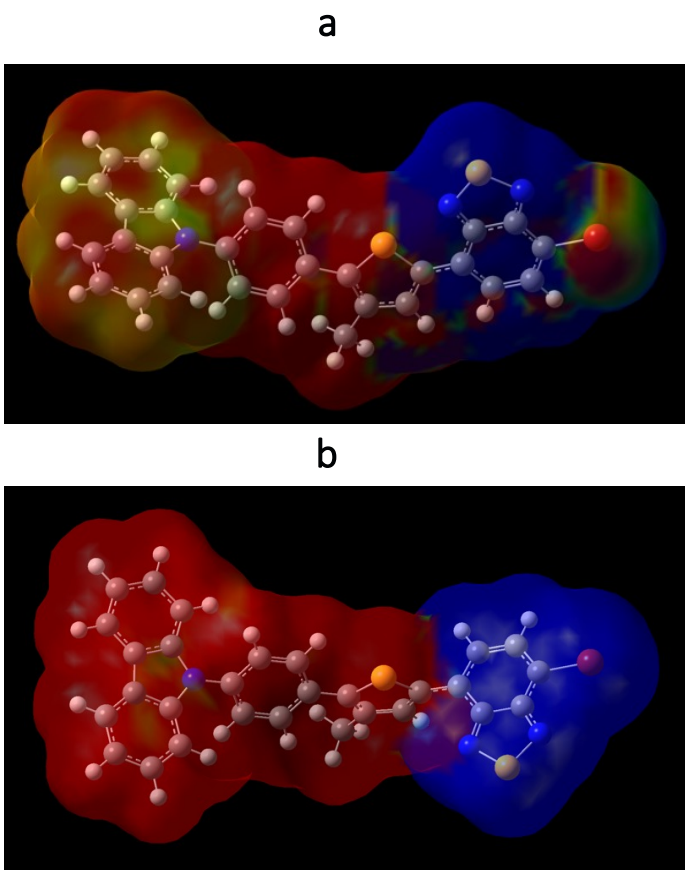

Figure 34 Electron density difference between excited state and ground state onto the SCF electron density surface for CBB in acetone when dihedral angle 3, θ_3, is at (a) 0 ° (b) 90°

Chapter 5

5.1. Conclusion

In our study of CBB, a complex organic dye molecule, both theoretical and experimental methods are employed to investigate photochemistry. The causes of fluorescence emissions are revealed by combining excitation-emission-matrix (EEM) and absorption spectroscopy. This method has demonstrated a direct correlation between the emission spectra of electronically excited states and the relationship between molecular structure and the dynamic solvent environment.

The subject of our study is the complex molecule carbazole-bromobenzothiadiazole (CBB). The fluorescence responses of CBB to solvent polarity and solvent viscosity are carefully examined using an EEM fluorometer. The fluorescence emission wavelength is constant when exposed to changes in solvent viscosity. However, the emitted light has a wavelength-shift when the solvent polarity is changed. In the present case, all excited states produce the same solvent-dependent emission spectrum, indicating that all access the same S_1 minimum from which the radiative decay occurs. Initially, it was believed that the observed solvatochromic shift might be attributed to a Twisted Intramolecular Charge Transfer state. However, extensive analysis using experimental and quantum-chemical computations has revealed that this is not the case. Our ab initio determination for assessing the solvatochromic shifts of acetone and toluene appears to be very accurate, although the agreement between theory and experiment within 10 cm^{-1} is likely fortuitous.

While our experimental observations are fully consistent with a previous study, a different understanding of the excited state dynamics is obtained. Our scan of the excited state PES reveals not only that the S_1 minimum is close to the Franck-Condon region and accessible without a barrier, but also that the previously proposed TICT minimum only exists when stabilized in a solvent environment and then, at a much higher energy compared to the LE minimum. The previous misassignment of the S_1 minimum as a TICT state is understandable since both the TICT and LE minima exhibit a large solvatochromic shift. The assignment of the excited state minimum is in our case guided by TD-DFT calculations of the S_1 state since the experimental evidence is inconclusive.

When performing calculations on TICT states we recommend using the natural transition orbitals, NTOs, and the calculated excited state dipole vector to help assign the state from which fluorescence occurs as either the charge transfer state having a large dipole along the donor-

acceptor axis, or the locally excited (LE) state with a dipole that is not necessarily aligned along the donor-acceptor axis. NTOs provide insights about the changes in electronic structure upon excitation that are difficult to obtain by only inspecting the canonical molecular orbitals.

Based on these arguments it is evident that not every large molecule exhibiting a solvatochromic shift can be classified as a Twisted Intramolecular Charge Transfer (TICT) molecule. The solvatochromic shift observed in such molecules can be partially attributed to the induced dipole moment imposed by the solvent. The solute is subjected to a large electric field in polar environments, leading to increased charge separation and a resulting larger dipole moment.

Computational studies provide valuable insights, but some limitations hinder the complete assessment of excited state properties. In this project, the effect of polarity of solvent and dipole moment changes of solute are evaluated but the polarizability effect of the solute could not be calculated. Polarizability calculations in the excited state require frequency information, which is computationally expensive and slow to obtain.

The other limitation of the calculation is the solvent model. The solvent model is not sufficient to determine the accurate radius of the cavity of the solute. This problem causes a difference via the Lippert-Mataga equation between the experimental and the computational data.

Future studies could improve our understanding of excited state properties and enable more precise predictions of solvatochromic shifts by examining other computational methods and improving solvent models.

More fundamentally, our study raises some concerns about the many molecules that have been previously described as having excited TICT state. If their classification is solely based on experimentally obtained solvatochromic shifts and calculated, canonical MOs their classification may be incomplete or even wrong.

5.2. Future work

During this research, we proved conventional knowledge and illuminated the underlying mechanisms of a crucial aspect of solvatochromism in organic dyes. This opens exciting opportunities for future investigations and applications.

We suggest reassessing a number of organic dyes, which have been long associated with solvatochromism drove by Twisted Intramolecular Charge Transfer (TICT) states. We can systematically revisit these dyes, identify the true nature of their solvatochromic behaviour, and

make a valuable contribution to a more precise understanding of their photophysical properties, equipped with our computational chemistry methods and experimental data.

Moreover, our results could prove to be a valuable reference for organic chemists working on fluorescent dye design. This research refutes the accepted view that the best way to produce a large dipole moment in a molecule is to simply lengthen the distance between the donor and acceptor groups. Despite our initial expectation of a significant charge separation, our observations, as shown in the case of CBB, revealed a small dipole moment change from 3 to 9 Debye during excitation.

In addition, our research suggests that the deliberate and strategic selection of functional groups to enhance the TICT probability within a molecule can be a challenging yet immensely promising approach. By tailoring the specific functional groups in a molecule, we can manipulate the electron distribution and molecular geometry to favor the occurrence of TICT states. This opens up exciting opportunities for designing molecules with tunable solvatochromic properties, making them highly adaptable to a range of environmental conditions.

This methodology encourages us to investigate the complicated interactions among excited states, electron delocalization, and functional groups. In the end, it gives organic chemists a new set of tools to create molecules with customized optical responses, expanding possibilities for applications in fields like imaging and sensors.

In conclusion, the prospects for more research in this field are exciting and promising, providing fresh perspectives on already-known substances and a singular chance to create novel approaches to organic dye molecular design. Anticipating an exciting future in organic chemistry, I'm excited about the potential influence my work may have.

References

1. Chernick ET, Abdollahi MF, Tabasi ZA, Junge MJ, Zhao Y. Study of a carbazole–bromobenzothiadiazole derived fluorescent molecular rotor: crystal structure, redox activity, and solvatofluorochromic effects. New Journal of Chemistry. 2022;46(2):572-81.
2. Guido C, Caprasecca S. Corrected Linear Response State-specific correction to solvent polarization response. Molecolab: Pisa; 2016.
3. Tian X, Murfin LC, Wu L, Lewis SE, James TD. Fluorescent small organic probes for biosensing. Chemical Science. 2021;12(10):3406-26.
4. Kodaimati MS, McClelland KP, He C, Lian S, Jiang Y, Zhang Z, et al. Viewpoint: Challenges in Colloidal Photocatalysis and Some Strategies for Addressing Them. Inorganic Chemistry. 2018;57(7):3659-70.
5. Zhang X-Y, Yang Y-S, Wang W, Jiao Q-C, Zhu H-L. Fluorescent sensors for the detection of hydrazine in environmental and biological systems: Recent advances and future prospects. Coordination Chemistry Reviews. 2020;417:213367.
6. Yang R, Zhu T, Xu J, Zhao Y, Kuang Y, Sun M, et al. Organic Fluorescent Probes for Monitoring Micro-Environments in Living Cells and Tissues. Molecules. 2023;28(8):3455.
7. Möckl L, Lamb DC, Bräuchle C. Super-resolved fluorescence microscopy: nobel prize in chemistry 2014 for eric betzig, stefan hell, and william e. moerner. Angewandte Chemie International Edition. 2014;53(51):13972-7.
8. Wang C, Chi W, Qiao Q, Tan D, Xu Z, Liu X. Twisted intramolecular charge transfer (TICT) and twists beyond TICT: from mechanisms to rational designs of bright and sensitive fluorophores. Chemical Society Reviews. 2021;50(22):12656-78.
9. Sung YM, Kwon ES, Maruyama YM, Shin Y, Ihn S-G, Kim JS, et al. Probing twisted intramolecular charge transfer of pyrene derivatives as organic emitters in OLEDs. Physical Chemistry Chemical Physics. 2022;24(36):21995-9.
10. Tharmaraj V, Pitchumani K. An acyclic, dansyl based colorimetric and fluorescent chemosensor for Hg(II) via twisted intramolecular charge transfer (TICT). Analytica Chimica Acta. 2012;751:171-5.
11. Fonseca T, Kim HJ, Hynes JT. Dynamics of twisted intramolecular charge transfer complexes in polar solvents. Journal of Molecular Liquids. 1994;60(1):161-200.
12. El-Zohry AM, Orabi EA, Karlsson M, Zietz B. Twisted Intramolecular Charge Transfer (TICT) Controlled by Dimerization: An Overlooked Piece of the TICT Puzzle. The Journal of Physical Chemistry A. 2021;125(14):2885-94.
13. Sasaki S, Drummen GP, Konishi G-i. Recent advances in twisted intramolecular charge transfer (TICT) fluorescence and related phenomena in materials chemistry. Journal of Materials Chemistry C. 2016;4(14):2731-43.
14. Kuimova MK, Yahioglu G, Levitt JA, Suhling K. Molecular Rotor Measures Viscosity of Live Cells via Fluorescence Lifetime Imaging. Journal of the American Chemical Society. 2008;130(21):6672-3.
15. Grabowski ZR, Rotkiewicz K, Siemiarczuk A. Dual fluorescence of donor-acceptor molecules and the Twisted Intramolecular Charge Transfer (TICT) states. Journal of Luminescence. 1979;18-19:420-4.

16. Lakowicz JR. Principles of Fluorescence Spectroscopy: Springer US; 2007.
17. del Valle JC, Catalán J. Kasha's rule: a reappraisal. Physical Chemistry Chemical Physics. 2019;21(19):10061-9.
18. Schweizer T, Kubach H, Koch T. Investigations to characterize the interactions of light radiation, engine operating media and fluorescence tracers for the use of qualitative light-induced fluorescence in engine systems. Automotive and engine technology. 2021;6(3-4):275-87.
19. Schweizer T, Kubach H, Koch T. Investigations to characterize the interactions of light radiation, engine operating media and fluorescence tracers for the use of qualitative light-induced fluorescence in engine systems. Automotive and Engine Technology. 2021;6(3):275-87.
20. Skoog DA, Holler FJ, Crouch SR. Principles of Instrumental Analysis. Seventh edition. ed. Boston: Cengage Learning; 2018.
21. Gomes AJ, Lunardi CN, Rocha FS, Patience GS. Experimental methods in chemical engineering: Fluorescence emission spectroscopy. The Canadian Journal of Chemical Engineering. 2019;97(8):2168-75.
22. Atkins PW, Friedman R. Molecular quantum mechanics. 4th / Peter Atkins, Ronald Friedman. ed. New York: Oxford University Press; 2005.
23. Cooksy A. Physical Chemistry: Quantum Chemistry and Molecular Interactions: Pearson; 2014.
24. Divac VM, Šakić D, Weitner T, Gabričević M. Solvent effects on the absorption and fluorescence spectra of Zaleplon: Determination of ground and excited state dipole moments. Spectrochimica Acta Part A: Molecular and Biomolecular Spectroscopy. 2019;212:356-62.
25. Lewis GN, Kasha M. Phosphorescence and the Triplet State. Journal of the American Chemical Society. 1944;66(12):2100-16.
26. Characteristics of Fluorescence Emission. Molecular Fluorescence2012. p. 53-74.
27. Environmental Effects on Fluorescence Emission. Molecular Fluorescence2012. p. 109-40.
28. Andrews NLP, Ferguson T, Rangaswamy AMM, Bernicky AR, Henning N, Dudelzak A, et al. Hadamard-Transform Fluorescence Excitation-Emission-Matrix Spectroscopy. Anal Chem. 2017;89:8554.
29. Abrahart EN. Dyes and their intermediates. 2nd ,1st American ed. New York: Chemical Pub.; 1977.
30. Lee J, Kim D, Kim T. Synthesis of Vapochromic Dyes Having Sensing Properties for Vapor Phase of Organic Solvents Used in Semiconductor Manufacturing Processes and Their Application to Textile-Based Sensors. Sensors. 2022;22(12):4487.
31. Amimoto K, Kawato T. Photochromism of organic compounds in the crystal state. Journal of Photochemistry and Photobiology C: Photochemistry Reviews. 2005;6(4):207-26.
32. Klymchenko AS. Solvatochromic and Fluorogenic Dyes as Environment-Sensitive Probes: Design and Biological Applications. Accounts of Chemical Research. 2017;50(2):366-75.
33. Levine I. Physical Chemistry: McGraw-Hill Publishing; 2008.
34. Gupta VP. Principles and Applications of Quantum Chemistry: Elsevier Science; 2015.
35. Young D. Computational Chemistry: A Practical Guide for Applying Techniques to Real World Problems: Wiley; 2004.
36. Grauso L, Teta R, Esposito G, Menna M, Mangoni A. Computational prediction of chiroptical properties in structure elucidation of natural products. Natural Product Reports. 2019;36(7):1005-30.

37. Tawada Y, Tsuneda T, Yanagisawa S, Yanai T, Hirao K. A long-range-corrected time-dependent density functional theory. The Journal of Chemical Physics. 2004;120(18):8425-33.
38. Yanai T, Tew DP, Handy NC. A new hybrid exchange–correlation functional using the Coulomb-attenuating method (CAM-B3LYP). Chemical Physics Letters. 2004;393(1):51-7.
39. Limacher PA, Mikkelsen KV, Lüthi HP. On the accurate calculation of polarizabilities and second hyperpolarizabilities of polyacetylene oligomer chains using the CAM-B3LYP density functional. The Journal of Chemical Physics. 2009;130(19).
40. Okuno K, Shigeta Y, Kishi R, Miyasaka H, Nakano M. Tuned CAM-B3LYP functional in the time-dependent density functional theory scheme for excitation energies and properties of diarylethene derivatives. Journal of Photochemistry and Photobiology A: Chemistry. 2012;235:29-34.
41. Cai Z-L, Crossley MJ, Reimers JR, Kobayashi R, Amos RD. Density Functional Theory for Charge Transfer: The Nature of the N-Bands of Porphyrins and Chlorophylls Revealed through CAM-B3LYP, CASPT2, and SAC-CI Calculations. The Journal of Physical Chemistry B. 2006;110(31):15624-32.
42. Zielinski TJ, Swift ML. Using Computers in Chemistry and Chemical Education: American Chemical Society; 1997.
43. Caricato M, Mennucci B, Tomasi J, Ingrosso F, Cammi R, Corni S, et al. Formation and relaxation of excited states in solution: A new time dependent polarizable continuum model based on time dependent density functional theory. The Journal of Chemical Physics. 2006;124(12).
44. Cammi R, Corni S, Mennucci B, Tomasi J. Electronic excitation energies of molecules in solution: State specific and linear response methods for nonequilibrium continuum solvation models. The Journal of Chemical Physics. 2005;122(10).
45. Shoute LCT. Dual fluorescence of 4,4′-bis(dimethylamino)benzophenone. Effects of specific and nonspecific interaction on the formation of twisted intramolecular charge transfer. Chemical Physics Letters. 1992;195(2):255-61.
46. Wang C, Qiao Q, Chi W, Chen J, Liu W, Tan D, et al. Quantitative design of bright fluorophores and AIEgens by the accurate prediction of twisted intramolecular charge transfer (TICT). Angewandte Chemie. 2020;132(25):10246-58.
47. Reichardt C. Solvatochromic dyes as solvent polarity indicators. Chemical reviews. 1994;94(8):2319-58.
48. Zielinski TJ, Harvey E, Sweeney R, Hanson DM. Quantum States of Atoms and Molecules. Journal of Chemical Education. 2005;82(12):1880.
49. Ottani S, Vitalini D, Comelli F, Castellari C. Densities, Viscosities, and Refractive Indices of Poly(ethylene glycol) 200 and 400 + Cyclic Ethers at 303.15 K. Journal of Chemical & Engineering Data. 2002;47(5):1197-204.
50. Sarode AV, Kumbharkhane AC. Dielectric relaxation study of poly(ethylene glycols) using TDR technique. Journal of Molecular Liquids. 2011;164(3):226-32.
51. Ohkuma S, Poole B. Fluorescence probe measurement of the intralysosomal pH in living cells and the perturbation of pH by various agents. Proc Natl Acad Sci U S A. 1978;75(7):3327-31.
52. Rumble J. CRC Handbook of Chemistry and Physics: CRC Press; 2023.
53. Lee S-C, Heo J, Woo HC, Lee J-A, Seo YH, Lee C-L, et al. Fluorescent Molecular Rotors for Viscosity Sensors. Chemistry – A European Journal. 2018;24(52):13706-18.

54. Hehlen MP, Brik MG, Krämer KW. 50th anniversary of the Judd–Ofelt theory: An experimentalist's view of the formalism and its application. Journal of Luminescence. 2013;136:221-39.
55. Frisch MJ, Trucks GW, Schlegel HB, Scuseria GE, Robb MA, Cheeseman JR, et al. Gaussian 16 Rev. C.01. Wallingford, CT2016.
56. Onsager L. Electric Moments of Molecules in Liquids. Journal of the American Chemical Society. 1936;58(8):1486-93.
57. Mukherjee S, Chattopadhyay A, Samanta A, Soujanya T. Dipole moment change of NBD group upon excitation studied using solvatochromic and quantum chemical approaches: Implications in membrane research. The Journal of Physical Chemistry. 1994;98(11):2809-12.
58. Demissie EG, Mengesha ET, Woyessa GW. Modified solvatochromic equations for better estimation of ground and excited state dipole moments of p-aminobenzoicacid (PABA): Accounting for real shape over hypothetical spherical solvent shell. Journal of Photochemistry and Photobiology A: Chemistry. 2017;337:184-91.
59. Sıdır İ, Sıdır YG, Berber H, Demiray F. Emerging ground and excited state dipole moments and external electric field effect on electronic structure. A solvatochromism and theoretical study on 2-((phenylimino)methyl)phenol derivatives. Journal of Molecular Liquids. 2015;206:56-67.
60. Ghanadzadeh Gilani A, Hosseini SE, Moghadam M, Alizadeh E. Excited state electric dipole moment of nile blue and brilliant cresyl blue: A comparative study. Spectrochimica Acta Part A: Molecular and Biomolecular Spectroscopy. 2012;89:231-7.
61. Suppan P, Tsiamis C. Absolute excited state dipole moments from solvatochromic shifts. Spectrochimica Acta Part A: Molecular Spectroscopy. 1980;36(11):971-4.
62. München L-M-U. The Onsager Reaction Field Model [Available from: https://www.cup.uni-muenchen.de/oc/zipse/teaching/computational-chemistry-2/topics/the-onsager-reaction-field-model/.
63. Divac VM, Šakić D, Weitner T, Gabričević M. Solvent effects on the absorption and fluorescence spectra of Zaleplon: Determination of ground and excited state dipole moments. Spectrochim Acta A Mol Biomol Spectrosc. 2019;212:356-62.
64. Andrews NL, MacLean AG, Saunders JE, Barnes JA, Loock HP, Saad M, et al. Quantification of different water species in acetone using a NIR-triple-wavelength fiber laser. Opt Express. 2014;22(16):19337-47.
65. Baumann W, Bischof H, Fröhling JC, Brittinger C, Rettig W, Rotkiewicz K. Considerations on the dipole moment of molecules forming the twisted intramolecular charge transfer state. Journal of Photochemistry and Photobiology A: Chemistry. 1992;64(1):49-72.
66. Martin RL. Natural transition orbitals. The Journal of Chemical Physics. 2003;118(11):4775-7.